The Development of a Denoising Model for LODOX® Statscan® Images

A Phantom Study

UNIVERSITY OF CAPE TOWN
DEPT. OF ELECTRICAL ENGINEERING

Presented by:

Travimadox Webb

Prepared for:

Dr. Yaaseen Martin(Supervisor)

Dr. Lindie Du Plessis(Co-supervisor)

September 14, 2024

Submitted to the Department of Electrical Engineering at the University of Cape Town in partial fulfilment of the academic requirements for the degree of Bachelor of Science degree in Electrical and Computer Engineering.

Abstract

In this work we describe a novel Thesis Template, to be used by students in Electrical & Engineering at the University of Cape Town. This section entails the abstract of the document.

Coming soon

Acknowledgments

I would like to thank The MasterCard Foundation for funding my four-year undergrad degree, enabling me to achieve my lifelong dream of becoming an engineer. With their financial support and mentorship, I have been able to achive this dream.

Words cannot express my gratitude to my supervisor, Dr. Yaaseen, for his invaluable patience and feedback on Machine Learning and Digital Signal Processing techniques for image processing. I also could not have undertaken this journey without my co-supervisor, Dr Lindie, who generously provided knowledge and expertise in Medical Imaging Technologies to enable me to complete this thesis successfully.

I am also grateful to my classmates and cohort members, especially my friends Clifford and Thikazi, for their constant emotional support, late-night feedback sessions, and moral support. Thanks should also go to the biomedical lab technical officer from the university, who guided me closely in learning how to use the Lodox technology.

Lastly, I would be remiss in not mentioning my family, especially my parents, Daniel and Violet, and siblings, namely Carlsberg, Bevy and Brasil. Their belief in me has kept my spirits and motivation high during this process.

Declaration

1. I know that plagiarism is wrong. Plagiarism is to use another's work and pretend that it is one's own.
2. I have used **IEEE** for citation and referencing. Each contribution to, and quotation in, this report from the work(s) of other people has been attributed, and has been cited and referenced.
3. This report is my own work, and is in my own words except where I have used quotations.
4. I have not paid a third party to complete my work on my behalf. My use of artificial intelligence software has been limited to **grammar mistakes correction, cohesion** and **clarity suggestions**.
5. I have not allowed and will not allow anyone to copy my work with the intention of passing it off as his or her own work.
6. I acknowledge that copying someone else's assignment or essay, or part of it, is wrong, and declare that this is my own work.

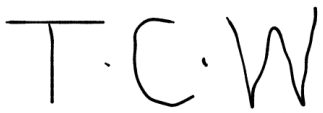

Travimadox Webb

September 14, 2024

Word Count:

12168 (errors:1) words

Glossary

Anscombe transform A variance-stabilizing transformation used to approximate the distribution of Poisson-distributed data by a normal distribution, often applied in image processing and statistics.. 9, 13, 15

DICOM Digital Imaging and Communications in Medicine (DICOM) is a standard for handling, storing, transmitting, and viewing medical imaging information. It enables the integration of medical imaging devices, such as scanners and servers, and ensures interoperability between different systems and institutions. DICOM defines both the image formats and the protocols for communication, making it essential in modern medical imaging environments, including radiology and cardiology.. 24, 33, 35

FBPconvNet A convolutional neural network architecture designed for improving image reconstruction in CT scans. It builds upon the traditional Filtered Back Projection (FBP) method by introducing convolutional layers that enhance image quality, particularly in low-dose CT images. FBPconvNet focuses on reducing artifacts and noise while preserving essential image details.. 20

FBPTransNet A neural network architecture that enhances image quality in CT scans by replacing the maximum pooling layers of FBPconvNet with Transformer modules. FBPTransNet features dual inlets and outlets to simultaneously process high and low energy CT images, and employs a multi-head attention mechanism to effectively model noise maps and recover fine texture details in the denoised images.. 20

golden hour term often used in trauma or emergency care to suggest that an injured or sick person must receive definitive treatment within the first 60 minutes from the time of injury or appearance of symptoms. 1

Staircase effect An artifact in digital imaging where smooth gradations of intensity are represented by abrupt steps or bands, rather than a continuous transition. This effect is commonly observed in images with low bit depth or when using inadequate interpolation methods.. 10

U-Net A type of convolutional neural network architecture primarily used for image segmentation tasks. It consists of an encoder-decoder structure with skip connections, enabling precise localisation and efficient learning from limited data. U-Net is widely used in medical image analysis due to its ability to produce accurate segmentation even with small training datasets.. xiii, 19, 20, 28–30, 33

Yaroslavsky filter A type of neighbourhood filter used in image processing for denoising images. It averages pixel values in a neighborhood but only includes those with similar intensity to the central pixel, effectively reducing noise while preserving edges. This method is computationally efficient and commonly used in fields like medical imaging and photography.. 16

Acronyms

ADF Anisotropic Diffusion Filter. 10

ASIC application-specific integrated circuits. 6

ASO Atom Search Optimization. 13

ATV Adaptive Total Variation method. 11

AWGN Additive White Gaussian Noise. 7, 9

BF Bilateral Filter. 10, 13

BM3D Block Matching and 3D filtering. 13–18, 20, 23

BRISQUE Blind/Referenceless Image Spatial Quality Evaluator. 12, 37

CCD Charge Coupled Detector. 1, 8

CNN Convolutional Neural Networks. xi, 17, 19, 20, 27, 28, 30, 32

CNR Contrast to Noise Ratio. 12

COV Coefficient of Variation. 12

CT Computed Tomography. 1, 2, 19, 20, 25

DnCNN denoising convolutional neural networks. 18

DSP Digital Signal Processing. 10, 20

DTCWT dual tree complex wavelet transform. 13, 14

FIR finite impulse response. 13

FNLM Fast Non-Local Means. 11, 12

GPU Graphical Processing Unit. 17

GUI Graphical User Interface. 22, 24

HNIPM Hybrid Non-iterative Poisson Model. 15

IBS improved threshold shrinkage. 14

ICA Independent Component Analysis. 16

LPA-RICI Local Polynomial Approximation - Relative Intersection of Confidence Intervals. 16

ML Machine Learning. 17, 20, 29

MMI Multiscale Multiplicative Innovations. 13

MRI Magnetic Resonance Imaging. 20, 24

MROF Modified Rudin-Osher-Fatemi model. 11

MS-VST multiscale variance stabilizing transform. 13, 15

MSE Mean Squared Error. 12, 13, 22, 28

N2N Noise2Noise. xi, xiii, 17, 18, 20–22, 24, 25, 27–31, 33, 38

N2V Noise2Void. xi, xiii, 17, 18, 20–22, 24, 25, 27, 28, 30, 32–34, 38

NIQE Natural Image Quality Evaluator. 12, 36

NLM Non-Local Means. xiv, 11–13, 15, 16, 20, 23

NNPS Normalized Noise Power Spectrum. 12

PCA Principal Component Analysis. 15, 17

PCCT Photon-counting CT. 15

PCD Photon Counting Detector. 1, 2, 6, 8, 19, 21

PIQE Perception-based Image Quality Evaluator. 37

PKAID-Net prior knowledge-aware iterative denoising neural network. 19

PRBF Poisson Reducing Bilateral Filter. 10

PSNR Peak Signal-to-Noise Ratio. 18, 22, 23, 36, 38

PURE-LET Poisson Unbiased Risk Estimation – Linear Expansion of Thresholds. 13

R-L Richardson-Lucy algorithm. 11

ROF Rudin-Osher-Fatemi model. 10, 11

SNR Signal-to-Noise Ratio. 22, 23, 36, 38

SSIM Structural Similarity Index Measure. 22, 24, 36, 38

TV Total Variation. xiv, 10, 11, 19, 20

UV Ultraviolet rays. 5

VMI Virtual Monoenergetic Images. 19

VST Variance Stabilising Transform. 9

WNNM Weighted nuclear norm minimization. 18

Contents

List of Figures

List of Tables

List of Equations

Nomenclature

Anscombe transform A variance-stabilizing transformation used to approximate the distribution of Poisson-distributed data by a normal distribution, often applied in image processing and statistics.. 9, 13, 15

DICOM Digital Imaging and Communications in Medicine (DICOM) is a standard for handling, storing, transmitting, and viewing medical imaging information. It enables the integration of medical imaging devices, such as scanners and servers, and ensures interoperability between different systems and institutions. DICOM defines both the image formats and the protocols for communication, making it essential in modern medical imaging environments, including radiology and cardiology.. 24, 33, 35

FBPconvNet A convolutional neural network architecture designed for improving image reconstruction in CT scans. It builds upon the traditional Filtered Back Projection (FBP) method by introducing convolutional layers that enhance image quality, particularly in low-dose CT images. FBPconvNet focuses on reducing artifacts and noise while preserving essential image details.. 20

FBPTransNet A neural network architecture that enhances image quality in CT scans by replacing the maximum pooling layers of FBPconvNet with Transformer modules. FBPTransNet features dual inlets and outlets to simultaneously process high and low energy CT images, and employs a multi-head attention mechanism to effectively model noise maps and recover fine texture details in the denoised images.. 20

golden hour term often used in trauma or emergency care to suggest that an injured or sick person must receive definitive treatment within the first 60 minutes from the time of injury or appearance of symptoms. 1

Staircase effect An artifact in digital imaging where smooth gradations of intensity are represented by abrupt steps or bands, rather than a continuous transition. This effect is commonly observed in images with low bit depth or when using inadequate interpolation methods.. 10

U-Net A type of convolutional neural network architecture primarily used for image segmentation tasks. It consists of an encoder-decoder structure with skip connections, enabling precise localisation and efficient learning from limited data. U-Net is widely used in medical image analysis due to its ability to produce accurate segmentation even with small training datasets.. xiii, 19, 20, 28–30, 33

Yaroslavsky filter A type of neighbourhood filter used in image processing for denoising images. It averages pixel values in a neighborhood but only includes those with similar intensity to the central pixel, effectively reducing noise while preserving edges. This method is computationally efficient and commonly used in fields like medical imaging and photography.. 16

Chapter 1

Introduction

1.1 Background

Timely and accurate diagnosis is a critical feature of trauma care as it directly impacts patients survival. Studies have shown that accurate information acquired during the golden hour is essential to saving patients' lives in trauma centres [1], [2]. One of the most important diagnostic tools in trauma care is medical imaging as it allows healthcare professionals to visualise internal body structures non-invasively. This gives accurate information on the extent of injuries enabling them to develop an effective prioritisation plan for the treatment phase. Among the many medical imaging technologies, X-ray remains one of the most widely used due to its rapid acquisition and cost-effectiveness compared to other medical imaging modalities [3]. However, traditional X-ray systems, while widely used, can delay the life-saving process in time-sensitive situations as it can take up to 8-48 minutes to get a full body scan [4].

Given the critical time delays associated with traditional X-ray systems, the need for a more efficient imaging solution becomes evident. The LODOX® Statscan® system offers a breakthrough, with its ability to produce full-body scans in under 13 seconds [4], [5], [6]. This represents a significant advancement in trauma care, particularly in scenarios where every second counts, such as mass trauma events [7], [8], [9]. Its reduced radiation dose further mitigates the risks associated with repeated imaging, making it a preferred choice in emergency settings [7].

Despite its advantages, the LODOX® Statscan® faces the challenge of high noise levels which comprises image quality. De Villiers showed that this increased noise is primarily due to the low X-ray dose used [10]. LODOX® has sought to improve this by replacing the Charge Coupled Detector (CCD) with Photon Counting Detector (PCD) [11]. While studies have shown that PCD technology does not increase noise in Computed Tomography (CT) scans [12], there is concern that its introduction

to LODOX® Statscan® systems may exacerbate the existing noise issue, potentially affecting diagnostic accuracy. This highlights the critical need for customised denoising algorithms for LODOX® Statscan® , which is the focus of this project.

1.2 Motivation

The increasing noise levels in LODOX® Statscan® images due to low X-ray dose pose a significant challenge to maintaining diagnostic accuracy [10]. Despite extensive research on denoising in traditional X-rays, CT scans, and ultrasound, the specific challenges posed by noise in LODOX® Statscan® images remain under-explored, creating a critical gap that this research aims to address. With the growing adoption of LODOX scanners in trauma centres worldwide [6], [13], the unresolved noise issues threaten to undermine the very benefits that make these scanners invaluable in emergency care. By developing an effective denoising model for LODOX® Statscan® images, this research not only seeks to enhance image clarity but also aims to ensure that the advantages of low-dose imaging do not come at the cost of diagnostic accuracy.

1.3 Problem Statement

The central research question is: "How can noise in Lodox Statscan images be effectively modelled and reduced while preserving their diagnostic quality and accuracy in trauma care?" Given the unique challenges of low-dose imaging and the incorporation of the PCD,this research aims to explore whether specialised denoising algorithms can be developed to overcome these issues. Although techniques like BM3D have proven effective in conventional CT scans [14], they may not be directly applicable to LODOX® Statscan® images due to the specific noise characteristics introduced by low-dose, highlighting the need for a customised approach.

1.4 Objectives

The main objective of this thesis is to develop a robust denoising model for Lodox Statscan images.

This can further be broken down into the following set objectives:

1. Review and compare existing denoising methods used in medical imaging, specifically X-ray imaging.
2. Adapt or develop new signal processing and/or machine learning techniques for noise reduction in LODOX® Statscan® images.
3. Validate the proposed model using imaging phantoms and determine optimal parameters for noise reduction.

4. Develop a user interface that goes along with the denoising algorithm to enable easy user access and use.

1.5 Thesis Contributions

The main contributions of this thesis are as follows:

1. A comprehensive review of current denoising techniques for medical imaging.
2. Development of a novel denoising model specifically designed for LODOX® Statscan® images.
3. Implementation and evaluation of the proposed model, demonstrating its effectiveness in reducing noise while preserving image quality.

1.6 Scope and Limitations

This project solely focuses on enhancing LODOX® Statscan® image quality by developing a custom denoising model using controlled non-anthropomorphic phantom studies, and it does not extend to clinical trials. The choice of non-anthropomorphic phantoms, including those provided by LODOX® and carefully selected everyday objects, is driven by their ability to simulate relevant imaging conditions while staying within project constraints. The exclusive focus on phantom studies limits the ability to translate findings to clinical practice directly, and additional validation in a clinical setting would be necessary to confirm the model's efficacy in real-world trauma scenarios. Additionally, given the model's design specifically for LODOX® Statscan® images, adaptation to other low-dose imaging systems may require additional tuning to accommodate different noise profiles. While these limitations confine the current study, they also highlight areas for future research, including clinical validation and the exploration of more comprehensive denoising models.

1.7 Thesis Outline

The remainder of this thesis is organized as follows:

Chapter 2, Literature Review: Reviews the theoretical foundations and related work in medical imaging and denoising techniques.

Chapter 3, Methodology: Details the research design, data collection methods, and the development of the denoising model.

Chapter 4, Design: Discusses the implementation of the denoising algorithms and the computational framework

Chapter 5, Results: Presents the findings from evaluating the denoising model.

Chapter 6, Conclusions: Summarizes the research contributions, discusses limitations, and suggests directions for future work.

Chapter 2

Literature Review

This chapter assesses existing medical imaging denoising techniques, specifically focusing on their applicability to LODOX® Statscan® images. It starts with a review of X-ray imaging theory, establishing a foundation to understand the unique challenges posed by LODOX® Statscan® system. After that, it delves into a discussion of the specific image artifacts associated with this technology. Finally, denoising algorithms used in Medical imaging are critically evaluated, assessing their suitability to LODOX® Statscan® images.

2.1 X-ray Imaging Fundamentals

This section summarises the theoretical framework and principles of X-ray imaging. Understanding the core principles of X-ray imaging is fundamental to improving the X-ray imaging quality through denoising, particularly in the context of low-dose systems like LODOX® Statscan®. The following subsections will look into mechanisms of X-ray production, X-ray detection and image formation.

The fundamental X-ray imaging theory, including X-ray generation, interaction with matter, and image formation, is extensively covered in [15], [16], [17], providing a solid foundation for the subsequent discussion.

2.1.1 X-ray Production

X-rays are generated in an X-ray tube by accelerating high kinetic energy electrons from the cathode across the electrostatic field in the vacuum towards the anode, striking the anode emitting X-rays.

X-ray emission is primarily controlled by the anode voltage, which dictates the maximum energy of the X-ray photons, and the tube current, which determines the photon flux. These parameters directly influence image quality by affecting the photon count detected by the X-ray detectors. Additionally, the focal spot size of the X-ray tube plays a crucial role in image resolution as it determines the size

of the X-ray beam. For instance, when the image details to be captured are smaller than the X-ray beam diameter, geometric blur is observed, which degrades image quality.

X-ray production is only one part of the imaging process; once generated, these Xrays must travel through various tissues, where their attenuation plays a critical role in the resulting image quality.

2.1.2 X-ray Attenuation

X-ray attenuation across various bodies is what brings about X-ray contrast. X-ray attenuation occurs when the X-ray photons collide with other atoms and get deflected from their path whilst losing some energy. The major forms of X-ray attenuation are Rayleigh Scattering, Compton Scattering, Photoelectric effect and pair production. These are summarised in the Table 2.1 below:

Interaction	**Photon Energy Range**	**Significance in Medical Imaging**
Rayleigh Scattering	Low Photon Energies	Negligible Above 50 keV thus negligible influence on image quality
Compton Scattering	All Photon Energies	Characteristic radiation leading to scattering that causes haze in the images.
Photoelectric Effect	50-70 keV	Crucial for X-ray contrast, especially at lower energies
Pair Production	Above 1.02 MeV	Limited relevance in medical imaging as rarely seen in practice

Table 2.1: Summary of Photon Interaction Mechanisms and Their Significance in Medical Imaging.

In LODOX® Statscan®, scattering is not an issue due to the unique detector architecture that reduces scattering by up to 95% [5]. As X-rays are attenuated as they pass through different tissues, this varying absorption information must be recorded to generate X-ray images. The following subsection will look into the X-ray detection and image formation mechanism and how it affects the image quality.

2.1.3 X-ray Detection and Image Formation

This subsection delves into how X-ray photons are converted and detected for imaging. X-ray intensity is primarily measured using photographic films and digital detectors, necessitating conversion to another energy form, usually visible light or Ultraviolet rays (UV) photons. Digital detectors are predominantly used today, as older photographic films and fluoroscope detectors were phased out due to their very low quantum efficiency and sensitivity.

During the conversion process, these digital detectors introduce various noise components, including electronic noise and quantum noise due to the use of application-specific integrated circuits (ASIC). In addition, converting X-ray photons into electrical signals can introduce image artifacts such as detector blur. Detector blur occurs due to the conversion layer, which typically emits visible light in all directions. A thick conversion layer increases the likelihood of cross-talk between neighbouring pixels, while a thinner conversion layer reduces this effect and lowers quantum efficiency. Keeping the conversion layer close to the detector element can help mitigate detector blur.

Motion blur is another significant factor impacting image quality, which arises when the patient moves during exposure due to breathing. High detector sensitivity and a high photon flux from the X-ray source can allow for shorter exposure times, which reduces the likelihood of motion blur affecting the final image.

2.2 Noise in X-ray imaging

This section will examine the various types of noise inherent in X-ray imaging, specifically low-dose X-ray imaging systems such as the LODOX® Statscan®. It then proceeds to discuss the sources of these noises in the LODOX® Statscan® and concludes with an analysis of the impact of the noise on image quality and diagnosis.

2.2.1 Types of Noise in X-ray Imaging

Noise is defined as random unwanted stochastic fluctuations and variations in brightness and colour information in an image [18], [19]. In X-ray, there are various noise types, each with a different statistical model arising from multiple sources such as the detectors' inherent properties, X-ray source, inspected objects and controller circuits [20], [21]. The primary noise present in X-rays is Quantum noise. Other prominent noise types include Electronic and Anatomical noise. These three noise types are discussed below:

Quantum Noise

Studies show that quantum noise is predominant in Photon Counting Detector (PCD) [21], [22]. Given that PCD are the detectors currently being used in the LODOX® Statscan® it is paramount to understand quantum noise. Quantum noise results primarily from X-ray photon detection and conversion [23], [20]. It is produced due to the random accumulation and distribution of the X-ray photons on the detectors' surface [21], [18], [24], [25], [3]. This is shown in the Figure 2.1 below:

Due to the wide spectrum energy of X-ray photons and the randomness mentioned above, quantum noise is modelled using the Poison distribution as shown below:

$$P(x) = e^{-\lambda t}\frac{(\lambda t)^k}{x!} \tag{2.1}$$

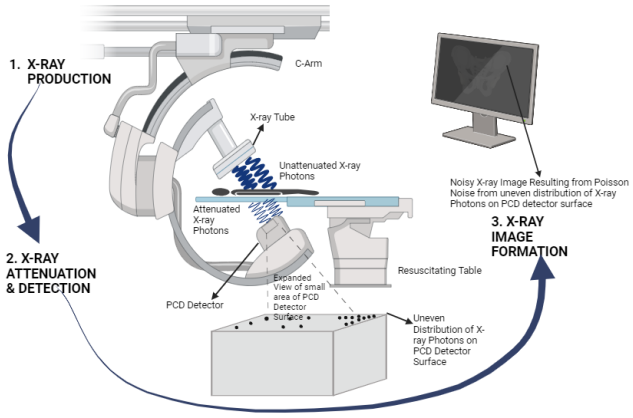

Figure 2.1: Diagram illustrating the generation of quantum noise in X-ray imaging due to the uneven distribution of X-ray photons on the PCD detector surface, resulting in a noisy image output. Created with BioRender.com

Where:

P(x): probability of distribution of photons
λ: Expected number of photons
X : measured number of photons
t : given time interval

Equation 2.1 depicts the signal-dependent nature of quantum noise, indicating it is not an additive noise like Additive White Gaussian Noise (AWGN) as shown in studies [26], [27], [25]. Since quantum noise follows Poisson distribution, the expected photon count (E(x)) is equal to the variance of the photon count(var(x)) over the given time interval in Equation 2.1. Thus quantum noise is proportional to the square root of the number of photons captured by the detector [25] and the square root of radiation exposure [22] as shown in equations 2.2 and 2.3 below:

$$\begin{aligned} E[x] = \text{var}[x] = \lambda t \\ \text{std}[x] = \sqrt{\lambda t} \end{aligned} \tag{2.2}$$

$$\sqrt{exposurelevel} \tag{2.3}$$

From the above, it can be deduced that by increasing the X-ray radiation and exposure time, quantum noise can be reduced [25]; however, this is not a suitable method in the LODOX® Statscan® system as it is inherently a low-dose X-ray system.

Electronic Noise

Electronic noise typically arises from random signals caused by thermal fluctuations in interconnected electronics [28], amplifier noise [29], and imperfections in detectors, such as thickness variations, scratches, and dust on the detector substrate [20]. Additionally, voltage variations over the long signal

distances in large detectors contribute to this noise [23]. This type of noise is prevalent in Charge Coupled Detector (CCD) [28] and is most pronounced at lower X-ray energy levels [18].

Electronic noise is modelled using the Gaussian distribution as shown in Equation 2.4 as it emanates from random signals [3]:

$$G(x) = \left(\frac{1}{\sigma\sqrt{2\pi}}\right) e^{-\frac{(x-\mu)^2}{2\sigma^2}} \tag{2.4}$$

Where:

σ: represents the standard deviation
X : represents the value of the pixel
μ : represents the mean

Since the LODOX® Statscan® now uses PCD instead of CCD, the impact of electronic noise is significantly reduced, with the primary source being the low X-ray doses used.

Anatomical Noise

Anatomical noise is caused by the projection of the 3D object of interest to a 2D plane, resulting in the overlapping of anatomical objects in the region of interest in the image [18], [20]. This overlap leads to local and global camouflaging that obstructs critical parts of the image [20] . Studies have shown that anatomical noise is particularly prevalent at very low X-ray energy levels [18]. Notably, anatomical noise is one of the most challenging to correct and affects all X-ray systems [20].

2.2.2 Impact of Noise on Image Quality and Diagnosis

Noise in X-ray systems significantly impacts image quality, particularly at low doses [18]. It can introduce obstructions that render images non-diagnostic [24]. Additionally, it can introduce artifacts that hinder the acquisition of quality images, potentially leading to false diagnoses [29]. Moreover, degradation in image quality makes visual interpretation difficult [30], [19] , complicating diagnostics for medical professionals [26]. Finally, the corruption of X-ray images due to noise further impairs diagnostic accuracy [25], [31] , [32] ultimately hindering effective clinical decision-making.

2.3 Denoising

From section 2.2.2, it has been established that noise degrades the image quality, thus making denoising a critical part of the pre-processing chain. The primary objective of denoising is to effectively suppress noise while preserving the image integrity [3], [19], [33]. Broadly, there are three X-ray denoising methods, as shown below:

1. **Use of customised hardware:** Done through incorporating hardware filters such as Aluminium filters in the X-ray machines to help reduce noise [34].

2. **Increase in X-ray dose:** An increase in the X-ray dose used significantly reduces the noise in the image. However, the dose is hindered by the Maximum Permissible Dose(MPD); thus, the dose cannot be arbitrarily increased [35].

3. **Digital Denoising Algorithms:** Involves using digital image processing algorithms to reduce the noise digitally.

Digital denoising algorithms are widely used as they are not as expensive as hardware customisation and do not increase radiation risk to the patients as the increasing X-ray dose method, thus making it the most effective technique to consider for denoising LODOX® Statscan® images.

The type of noise in the images significantly impacts the effectiveness of denoising algorithms, and studies caution against the assumption that all noise is AWGN [35]. As highlighted in Section 2.2.1, quantum noise is the most common in X-ray images, especially in low-dose settings. Consequently, noise-independent denoising algorithms do not work well on X-ray images, making Poisson-based methods the preferred approach [27], [36]. Studies have suggested two approaches to handle Poisson noise, as discussed below:

1. **Poisson Direct Denoising methods**: Model the Poisson noise statistics, which are usually helpful when the images suffer from very high noise levels [35], [36].

2. **Poisson Variance Stabilising Transform (VST) Denoising methods:** Involves transforming the Poisson noise to Gaussian noise because when the photon count is large enough, Poisson distribution approaches Gaussian, and the Anscombe transform is used to stabilising the variance of the Poisson noise [36].

However, denoising X-ray images presents several critical challenges discussed below:

1. **Maintaining flat regions:** Flat regions in the image must remain flat without introducing noise or artifacts [3].

2. **Preserving image boundaries:** Image boundaries must be retained without causing blurring [3].

3. **Protecting global contrast and textural features:** The global contrast should be preserved, and textural details should not be lost [19].

4. **Avoiding new artifacts:** The denoising process should not generate any new artifacts in the image [3], [27].

Over the years, various algorithms have been proposed to address these four challenges. These algorithms are generally classified into three broad categories: Classical Filters, Hybrid Filters and Deep learning methods [3], [35]. The following section will analyse each category in detail, exploring their advantages, disadvantages, and suitability for handling Poisson noise in the LODOX® Statscan®.

2.3.1 Classical Filters

This subsection briefly discusses the classical Digital Signal Processing (DSP) filters implemented to combat noise in X-ray Images, broadly classified into spatial and transform filters. Spatial filters are further categorised into linear and non-linear filters. Linear filters are easy to implement as they apply non-discriminate denoising to all the pixels without prior categorisation [26] and thus are not good with signal-dependent noise leading to artifacts and blurring [3], [37]. In contrast, non-linear filters first detect noisy pixels and then replace them selectively, making them more effective for denoising [26].

Spatial Domain Filters

This subsection discusses key spatial domain filters currently used for X-ray image denoising. A detailed analysis of these filters, outlining their strengths, weaknesses, and applicability to LODOX® Statscan® images, is discussed below.

Anisotropic Diffusion Filter (ADF) is a spatial diffusion filter that adaptively smooths images, preserving important anatomical structures by controlling diffusion across edges [25] . Although ADF effectively preserves micro-texture and edges, its performance degrades with larger mask sizes, reducing its ability to handle quantum noise [25] . Additionally, ADF is slow, and its effectiveness depends heavily on careful parameter selection, and when not done correctly it tends to remove some image details degrading image quality [3], [25] . Consequently, this makes ADF less suitable for the high levels of quantum noise in LODOX® Statscan® images.

Despite ADF's ability to maintain micro-texture and edges, its shortcomings in dealing with quantum noise in LODOX® Statscan® images make exploring alternative techniques, such as the Bilateral Filter (BF), necessary. BF is a non-iterative filter that merges grey levels of pixels based on their spatial and photometric similarity, preserving sharp structural patterns while suppressing noise [3], [25]. However, BF is prone to gradient reversal artifacts near edges, leading to a loss of fine detail [3], [25]. Kirti et al. [27], [38] attempted to address this by developing an enhanced version, Poisson Reducing Bilateral Filter (PRBF), adding the capability to remove Poisson Noise, although it still struggles with photon-limited images. Given that LODOX® Statscan® images are photon-limited, the BF may not be ideal for denoising.

Since BF struggles with photon-limited images, exploring other filters that can effectively handle quantum noise, such as Total Variation (TV) filters, is necessary. TV filter popularly known as Rudin-Osher-Fatemi model (ROF) was first developed by Rudin et al. [39] and is an edge-preserving algorithm designed to handle discontinuities in anatomical details [26], [40]. Studies show that TV is effective in denoising Poisson and Gaussian noise [40]; however, it struggles to preserve edges, produces the Staircase effect [40] and has long processing times [41]. Over time researchers have sought to address these challenges by improving the initial version of the TV algorithm. Some of these adaptions are summarised in Table 2.2 below:

Algorithm	Description	Challenges
Richardson-Lucy algorithm (R-L) and TV (Dey et al.) [42]	Combined R-L and TV to develop a Poisson-based denoising algorithm specifically suited for microscopy images.	Only Tailored for microscopy images
Modified Rudin-Osher-Fatemi model (MROF) (Triet et al.) [43]	An improved version of ROF that can process Poisson noise.	Long execution times, Artificial artifacts, Cannot handle photon-limited images.
Adaptive Total Variation method (ATV) (Prasath) [44]	Developed to address artificial artifacts in MROF.	Faces the same challenges as MROF.
Enhanced ATV (Liu et al.) [45]	Modified ATV to denoise photon-limited images.	Long execution times.

Table 2.2: Summary of Adaptations to TV Filters to addressing challenges in original TV filter.

Non-Local Means (NLM) has emerged as an alternative to denoise photon-limited images to address the shortcomings of TV filters. NLM uses a non-local averaging technique that operates on all similar pixels, removing noise after exploring redundant information [3], [26], [40]. Consequently, this leads to high detail preservation in images [40]. However, despite the high detail preservation, NLM suffers from slow execution time due to the computational overhead arising from the complexity of evaluating the pixel weights [3], [40]. Various researchers have proposed solutions to address the challenges, as summarised in Table 2.3 below:

Researcher(s)	Proposed Solution	Challenges Addressed
Mahmoudi and Sapiro [46]	Modified NLM by adding Preselection of neighborhoods	Increased speed
Pierrick Coupe [47]	Added parallel processing	Improved execution time
Deledalle et al. [48]	Modified NLM to incorporate Poisson noise statistics	Tailored for Poisson noise
Shim et al. [49]	Implemented Fast Non-Local Means (FNLM)	Significant speed improvement i.e 3.7 times faster than TV filter

Lee et al. [34]	Combined NLM denoising algorithm with Aluminium additive hardware filters	Superior results in Contrast to Noise Ratio (CNR), Coefficient of Variation (COV), Natural Image Quality Evaluator (NIQE), and Blind/Referenceless Image Spatial Quality Evaluator (BRISQUE)
Lee [41]	FNLM with acceleration function and Euclidean distance	Superior Normalized Noise Power Spectrum (NNPS), CNR, and COV values; fast processing time (0.17s)

Table 2.3: Summary of Proposed Solutions to Address Challenges in NLM Filter

NLM filters still suffer from slow execution due to computational complexity and require high-speed hardware to execute faster, thus limiting their suitability for denoising LODOX® Statscan® images.

Transform Domain Filters

This subsection details some transform domain filters used in X-ray image denoising. Unlike spatial filters, transform domain filters operate by converting the image into an alternative representation, such as the Wavelet or Fourier domain, where denoising is performed, after which the image is transformed back to the spatial domain using an inverse transform. A detailed analysis of these filters, outlining their strengths, weaknesses, and applicability to LODOX® Statscan® images, is discussed below.

Gaussian filter is the most widely used transform domain filter known for reducing edge blurring and computational efficiency; however, it loses a lot of image detail [3] , [26]. Given that Gaussian filter works is tailored for Gaussian noise, it struggles to denoise Poisson noise prevalent in LODOX® Statscan®. Researchers have opted for other transform domain filters to denoise X-ray images to address these shortcomings.

One of the filters that has shown promise in improving the shortcomings of the Gaussian filter is the wiener filter. It is an Mean Squared Error (MSE)-optimal stationary filter that balances noise smoothing and inverse filtering, using local image variance for adaptive smoothing [3], [25], [50]. Studies have shown that the wiener filter effectively reduces Gaussian impulse and speckle noise whilst preserving the edges [25], [51]. However, despite these advantages, it only provides a point estimate that gives optimal results under specific conditions, making it less effective in handling signal-dependent noises such as Poisson [3]. Additionally, it leads to blurry images due to the use of fixed kernel size [25].

Researchers have attempted to improve the Wiener filter to enhance its performance. For instance,

Goreke [52] modified a wiener filter by incorporating an finite impulse response (FIR) filter with Atom Search Optimization (ASO) optimisation, demonstrating its superiority over NLM, BF, Block Matching and 3D filtering (BM3D), Poisson Unbiased Risk Estimation – Linear Expansion of Thresholds (PURE-LET), Bayes, and dual tree complex wavelet transform (DTCWT) filters in terms of contrast index, entropy, sharpness, and computational efficiency. Additionally, Lahmiri [19] developed a multistep iterative Wiener filter where the denoised output from one step is the input to the next stage, stopping based on an energy condition and showed that it could denoise and restore the original texture in finite iterations. However, this approach was limited to Gaussian noise [19], reducing its applicability to other noise types. Despite these improvements, the Wiener filter still struggles to handle Poisson noise, making it a less suitable option for LODOX® Statscan® images, which are predominantly degraded by Poisson noise.

While the wiener filter preserves the image texture, its limitations in handling quantum noise suggest that complementary methods, such as wavelet filters, are necessary for optimal denoising. Primarily, wavelet filters operate by applying shrinkage or thresholding to wavelet coefficients, followed by image synthesis [40]. The local definition of features allows wavelet filters to preserve minute edges and details in X-ray images [3], [40]. Notably, wavelet filters are associated with challenges of estimating an appropriate threshold and the tendency to introduce artifacts leading to smooth edges at times [3], [40]. To address these challenges associated with the wavelet filter, researchers have developed various variations, which are summarised in Table 2.4 below:

Researcher(s)	**Method & Description**	**Strengths**	**Limitations**
Thierry et al. [53]	PURE-LET: Based on the unnormalised Haar wavelet transform, the minimisation of unbiased MSE estimate	Handles Poisson noise. Competitive in denoising and computational complexity	Cannot handle photon-limited images
Timmermann and Nowak [54]	Multiscale Multiplicative Innovations (MMI) Model: A simple Bayesian intensity estimate procedure	Denoises photon-limited images	Highly complex
Zhang et al. [55]	multiscale variance stabilizing transform (MS-VST): Extension of Anscombe transform combining wavelet, ridgelet, and curvelet	Denoises photon-limited images	Highly complex

Wang [51]	Adaptive Wavelet Wiener Filter: Pre-processing, three-wavelet decomposition using Daubechies wavelet (db5), improved threshold shrinkage (IBS)	Superior performance in preserving edges, enhancing image quality in low-dose X-ray and medical images	Highly complex
Kaur et al. [56]	Wavelet-Based Statistical: Uses realistic distribution of wavelet coefficients	Better feature preservation in medical images	Highly complex
Du et al. [57]	DTCWT: Dual-tree complex wavelet transform	Better than wavelet transform filters in Poisson noise reduction in X-ray images	Highly complex

Table 2.4: Summary of Wavelet Filter Variations for Poisson Noise Reduction in Medical and X-ray Images, Highlighting Strengths and Challenges

The wavelet filter has proven effective in denoising photon-limited images by preserving fine edges and details while reducing Poisson noise. Despite challenges such as determining the optimal threshold and potential edge smoothing, advanced variations like IBS techniques have enhanced its performance. These methods, particularly when using Daubechies wavelet (db5), demonstrate superior capability in handling low-dose X-ray images, making wavelet filters a potential denoiser for LODOX® Statscan® images.

2.3.2 Hybrid Filters

Hybrid filters have gained popularity for X-ray image denoising due to the non-adaptability of classical filters, as they are suited to handling specific types of noises. Hybrid filters include filters that combine two or more classical filters or use entirely non-classical spatial and transform methods to denoise the images. This subsection summarises the most notable hybrid filter approaches, strengths, and limitations.

One of the most successful hybrid filters is 3D transform domain filtering. These methods convert 2D images into 3D domain and apply a sliding window to process the blocks, matching similar regions to effectively reduce noise through shrinking coefficients in the 3D arrays [40]. The most widely used 3D domain filter is the BM3D, which is known for its significant noise reduction while preserving local texture information [25]. However, BM3D faces challenges when the image is heavily contaminated with noise, leading to overshooting, which can obscure the structural information in X-ray images [25].

Over time, researchers have developed various BM3D modifications to address the abovementioned challenges. For instance, Makitalo et al. [58] modified the BM3D for Poisson noise by incorporating an Anscombe transform to stabilise the variance of Poisson-corrupted images. Additionally, Harrison et al. [14] developed a custom version of BM3D specifically for Photon-counting CT (PCCT) scanners called BM3D_PCCT that uses four energy thresholds and exploits correlation and exact alignment between energy bins to denoise the images. They demonstrated that BM3D_PCCT achieved a 65.0% reduction in noise standard deviation, tighter clustering of attenuation values, and smaller mean angular differences compared to BM3D [14]. Ren [59] also developed a denoising method based on subspace decomposition, employing sparse representation and block matching to suppress noise. In simulations using a three-dimensional digital mouse phantom, Ren's method improved the peak signal-to-noise ratio by 2.21 dB compared to existing techniques when the photon flux was 4×10^3 [59].

Although BM3D is the most widely used hybrid filter, several other filters have been developed to address its shortcomings. However, most of these alternatives are not widely adopted. Table 2.5 below summarises these filters.

Researcher	**Hybrid Filter Method**	**Advantages**	**Limitations**
Salmon et al. [60]	Non-local Principal Component Analysis (PCA)	Better noise reduction compared to BM3D	Increased execution time due to iterative nature; struggles with noise detection in high-dimensional data.
Kipele [36]	PCA combined with NLM	Performs well in reducing noise in images with moderate intensity	Performance not tested for extreme Poisson noise levels.
Wensen et al. [61]	Hybrid Non-iterative Poisson Model (HNIPM) trained on Anscombe transform	Removes Poisson noise in both high and low-peak images	Long execution time; not suitable for photon-limited images.
Jisha & Suresh [62]	Anscombe transform with Curvelet and MS-VST	Performs better than most wavelet-based filters	Execution time may be high; tested on specific noise types.

Dong [32]	Wavelet filter combined with median filter	Preserves image details while reducing noise	Tested only on Gaussian and Salt-and-Pepper noise; efficacy on Poisson noise not verified.
Dabov et al. [63]	Non-local adaptive nonparametric filtering	Similar performance to NLM and Yaroslavsky filter	Limited testing on medical X-ray images; complex computational process.
He et al. [64]	Guided filter	Superior performance compared to bilateral filter; reduces quantum noise	Dependent on parameter selection and guidance image; large filter masks lead to blurring.
Treece et al. [65]	Bitonic filter	Effectively reduces noise without artifacts; good edge preservation	Can cause significant blurring if not carefully applied.
Mandic et al. [37]	Local Polynomial Approximation - Relative Intersection of Confidence Intervals (LPA-RICI) adaptive algorithm	Less execution time due to easy parallelisation	Limited testing on specific noise types.
Umadevi et al. [31]	Bi-orthogonal Haar wavelets with BayesShrink thresholding and Independent Component Analysis (ICA)	Achieves high-quality images quickly (PSNR = 44.85)	May not work as efficiently in photon-limited settings.
Kirti [35]	Hybrid filter combining non-local means and BM3D collaborative filtering	Encouraging results with Poisson noise; improved PSNR over wavelet-based methods	Execution time still an issue compared to faster filters.

Table 2.5: Summary of Hybrid Filters for X-ray Image Denoising

Hybrid filters have emerged as an effective solution for addressing the limitations of classical filters by

combining multiple techniques to handle different types of noise. These filters, such as those based on PCA, curvelet transforms, and adaptive models, show improved noise reduction, edge preservation, and execution efficiency. Notably, hybrid methods like adaptive wavelet Wiener preprocessing and variations of BM3D tailored for Poisson noise have demonstrated superior performance in enhancing image quality in medical X-ray imaging, making them well-suited for the complex noise characteristics present in LODOX® Statscan® images.

2.3.3 Deep Learning Methods

This subsection provides a brief overview of Machine Learning (ML) methods applied to medical imaging denoising, highlighting their advantages and associated challenges.

Machine learning, particularly deep learning, has transformed data processing by solving complex problems, including medical image denoising. Deep learning employs artificial neural networks to learn the characteristics of a given problem and develop effective solutions. In medical image denoising, ML models are trained to identify and remove noise patterns from the images. These models fall into two broad categories: supervised learning, which requires clean, labelled data (ground truth), and unsupervised learning, which does not require ground truth data. Unsupervised learning models are preferred as in clinical settings, acquiring noise-free data in medical imaging is impractical, except through simulations, which may not always accurately reflect real-world conditions [66].

The shift from conventional filters to ML methods has been driven by several challenges. Studies have shown that the manual selection of filters is a cumbersome process requiring good domain knowledge [3]. Additionally, many conventional filters rely on prior noise information, further complicating optimisation [3]. In contrast, ML methods require relatively few tuning parameters and learn by themselves to denoise images [67]. For instance, Convolutional Neural Networks (CNN) excel at extracting relevant features from noisy data and can be trained efficiently using parallel processing with Graphical Processing Unit (GPU)s [3]. This makes ML methods more efficient than conventional filters in many cases.

The following will explore several specific applications of deep learning frameworks that denoise X-ray images with a specific focus on unsupervised models. Noise2Noise (N2N) and Noise2Void (N2V) are the two most common unsupervised deep learning denoising methods that have been used in medical image denoising as they do not require clean reference images, making them well-suited for applications such as LODOX® Statscan® image denoising.

Lehtinen et al. [68] developed N2N to address the challenge of requiring clean and noisy image pairs during the model training phase. N2N makes use of two noisy images each with an independent noise distribution to learn the underlying signal from these noise-corrupted data points. Studies have shown N2N achieving comparable performance to models trained with clean images. For instance,

Lehtinen et al. [68] trained the N2N for 300 epochs with noisy targets and achieved an average Peak Signal-to-Noise Ratio (PSNR) of 31.10 dB on the validation set, while training with clean targets reached 31.14 dB, comparable to previous work by Wang et al. [69] and Lee et al. [70]. Additionally, N2N can generalise across various types of noise distributions [68]. The use of noisy image pairs during training and adapting to various noise types makes N2N a highly suitable model for denoising LODOX® Statscan® images where noise is prevalent and acquiring images is impossible.

Krull et al. [71] developed N2V to eliminate the need for paired noisy images during the training phase. N2V uses single noisy images to train the network to predict the values of randomly masked pixels, encouraging the model to learn spatial relationships in the data. This makes N2V highly adaptable to various noise types as minimal assumptions about the underlying noise distribution are made. Krull et al. [71] demonstrated N2V applicability to various imaging modalities by running experiments on photography, fluorescence microscopy, and cryo-Transmission Electron Microscopy. They concluded that as long as the assumptions of predictable signal and pixel-wise independent noise are met, N2V performance is comparable to traditional and N2N-trained models [71]. Since N2V does not require clean images or paired noisy images, it is a highly scalable solution, well-suited for LODOX® Statscan® images.

Both Noise2Noise and Noise2Void are promising models for medical image denoising due to their unsupervised nature, effectively addressing the challenges of acquiring clean training data in a clinical context like Lodox imaging.

Other attempts to denoise X-ray images primarily using supervised learning are summarised in Table 2.6 below:

Author(s)	Proposed Model	Strengths	Challenges
Zhang et al. [72]	denoising convolutional neural networks (DnCNN): Neural network that outputs residual noise (V) and computes clean X-ray (C) as the sum of noisy observation and residual image	Outperforms BM3D and Weighted nuclear norm minimization (WNNM)	Not effective for Poisson noise
Hariharan [66]	Learning-based model using model-based simulations and data-driven normalisation for robust denoising	Outperforms BM3D and WNNM; produces visually superior results	Limited clinical practicality due to reliance on simulated data

Nadkarni et al. [67]	Custom 2-D U-Net CNN for quick iterative reconstruction and accurate material decomposition across energy thresholds	15 times faster than iterative reconstruction; higher spatial resolution	Relies on supervised learning and high computational resources; training detector prone to distortions
Huber et al. [12]	CNN model using U-Net for ultra-high-resolution PCD Computed Tomography (CT), trained with image-based noise insertion	Retains fine details and low contrast signals; preferred by radiologists	Limited by supervised learning and high-quality training data requirements
Chang et al. [73]	prior knowledge-aware iterative denoising neural network (PKAID-Net) using prior knowledge-aware iterative denoising neural network using lower-noise Virtual Monoenergetic Images (VMI) for improved denoising	96% noise reduction; maintains spatial and spectral fidelity	Potentially complex iterative refinement may limit practical application
Baffour et al. [74]	CNN model for detecting multiple myeloma using PCD CT images	Enhanced detection of abnormalities; better clarity and accuracy	Focused on detection and denoising only a small subset
Durcos et al. [75]	Uses regularisation strategy to suppress noise	Easy to implement	Limited noise suppression effect across various noise types
Zhang et al. [76]	Third-Order Tensor Model that combines TV regularisation with tensor similarity and image sparsity	Improved noise suppression	High computational costs due to tensor reconstruction

Sun et al. [77]	FBPTransNet that combines U-Net CNN with Transformer module for improved image detail restoration	Outperforms TV and FBPconvNet; clearer image details	Does not clearly address Poisson noise

Table 2.6: Summary of Deep Learning Approaches for X-Ray Image Denoising

2.4 Conclusion

The literature review provided a comprehensive analysis of classical and modern denoising techniques, mainly focusing on their applicability to low-dose systems such as the LODOX® Statscan® systems.

The review began with a brief overview of X-ray imaging fundamentals, including X-ray production, attenuation, and detection and their significance to image quality. This was followed by an analysis of noise types in X-ray images. It was highlighted that the predominant noise degrading X-ray images is Poisson noise, and various Posison denoising methods were looked into. A plethora of classical DSP filters was looked into, highlighting their limitations in handling photon-limited images. Despite some variations of wavelet and NLM filters showing promise, they often fell short of effectively reducing Poisson noise without compromising image quality. The review then transitions to hybrid filters, particularly the BM3D. BM3D demonstrates significant improvement over classical filters but still faces challenges in denoising noise-heavy images such as LODOX® Statscan® images. This underscored the need for adaptable denoising methods to learn different noise patterns.

ML methods like N2N and N2V offer significant potential due to their ability to operate without clean training data. This is critical for LODOX® Statscan® as it is impossible to obtain ground truth data. However, in most of the literature, the testing was mostly done on Magnetic Resonance Imaging (MRI), CT and microscopy images, with limited application to low-dose X-ray systems like the LODOX® Statscan®. While N2N and N2V have shown adaptability across various noise types in other imaging domains, applying these models to the LODOX® Statscan® system presents both a challenge and an opportunity for further research. This project aims to bridge this gap by adapting and enhancing N2N and N2V models specifically for LODOX® Statscan® images, documenting the results and challenges encountered in this process. This approach addresses the current limitations in the literature and contributes to the development of more effective denoising techniques for low-dose X-ray imaging.

Chapter 3

Methodology

This chapter provides a detailed breakdown of the research procedures undertaken to compare the suitability of two deep learning models, Noise2Noise (N2N) and Noise2Void (N2V) as potential denoising models for the LODOX® Statscan®. It begins with an in-depth analysis of the user and functional requirements, followed by a detailed analysis of the research design. Theoretical background and analysis of N2N and N2V models are then addressed, after which an exploration of the various research instruments used to develop them, ranging from software to hardware tools is addressed. Data collection is then explored in detail, exploring the various phantoms used and the rationale behind their use. This is followed by analysing the performance evaluation metrics to evaluate the two models. The chapter culminates with an analysis of the limitations and ethical concerns associated with the study.

3.1 Model Development and Comparison Procedure

The methodology followed the waterfall approach and is broken down into the following phases and summarised in Figure 3.1 below:

1. **Literature Review and Familiarisation:** This phase involved an extensive review of existing medical imaging denoising techniques and learning the tools and technologies essential for the project. This included understanding the operational principles of the LODOX® Statscan® system, gaining familiarity with Photon Counting Detector (PCD) technology, and working with programming languages commonly used in denoising models, such as Python and MATLAB®.

2. **Data Collection and Pre-Processing:** This phase involved configuring the LODOX® Statscan® with the required parameters and scanning the selected phantoms. After scanning the phantoms, the images were exported through DVS® software for pre-processing, which included normalisation, data type conversion, and the addition of extra dimensions.

3. **Model Selection and Design:** This phase involved developing and implementing the suitable models identified in Phase 1, specifically N2V and N2N, due to their adaptability and ability to train without clean images. Variations of these models were implemented in Python programming language on the Google Colab cloud platform.

4. **Model Training and Validation:** The data set was split into a training(80%) set and a validation(20%) set. The models were trained in two stages. The first stage involved using ten training images over 50 epochs with 100 training steps per epoch. The second stage involved 29 images over 150 epochs with 100 training steps per epoch. After each phase, the training and validation loss and Mean Squared Error (MSE) were analysed to evaluate model generalisation, with hyperparameter tuning performed as needed.

5. **Model testing and evaluation:** In this phase, a new test set of 10 images not used in training was collected. These images were passed through the models, and performance metrics such as proxy Signal-to-Noise Ratio (SNR), Peak Signal-to-Noise Ratio (PSNR), and Structural Similarity Index Measure (SSIM) were calculated to assess the models' suitability for the LODOX® Statscan® system.

6. **Graphical User Interface (GUI) Development:** Once the model was tested and the results analysed, a GUI was created to enable easy denoising of the images using the two models. This GUI is a preliminary step for further integrating the denoising models into the LODOX® DVS® Software.

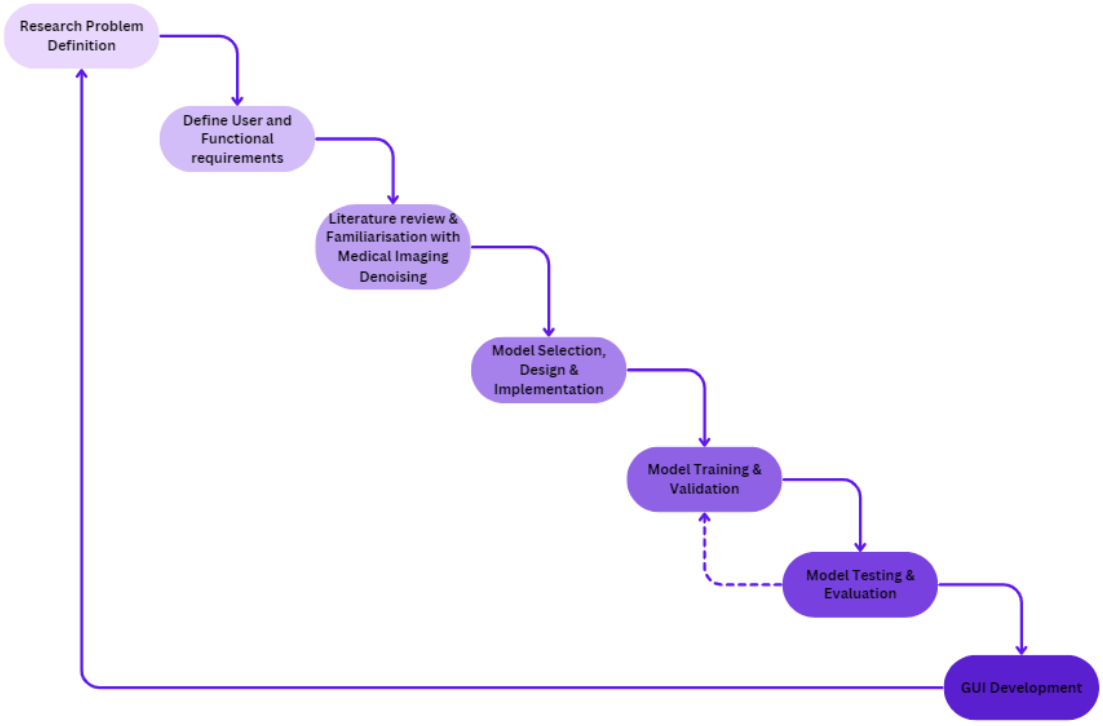

Figure 3.1: Waterfall models depicting the methodology overview

3.2 System Requirements

The user requirements for the system are detailed in Table 3.1 below:

Table 3.1: User Requirements

ID	Requirement	Description
UR-01	High Image Quality	The model should significantly enhance the clarity and quality of LODOX® Statscan® images.
UR-02	Retention of Anatomical Details	The model should preserve critical anatomical structures within the images.
UR-03	Compatibility with Existing Systems	The model should be compatible with existing medical imaging software and systems.
UR-04	Fast Processing Time	The model should process images quickly to support real-time diagnostic workflows.
UR-05	User-Friendly Interface	The model should provide an intuitive interface to apply the denoising model easily.
UR-06	Scalability	The model should handle varying image sizes and resolutions effectively.
UR-07	Robustness Across Noise Levels	The model should effectively reduce noise in images with varying noise intensity levels.
UR-08	Minimal Artifact Introduction	The model should minimise the introduction of artifacts during the denoising process.

These user requirements are then used to derive the functional requirements of the system which are then detailed in the Table 3.2 below:

3.3 Research Design

3.3.1 Familiarisation With Medical Imaging Denoising Techniques

Relevant literature detailing the various algorithms used in X-ray image denoising was explored, with a particular focus on methods that are effective in denoising photon-limited images with Poisson noise as the LODOX® Statscan® images meet that criterion. Deep learning methods were given precedence as they are adaptable across various noise types and outperform most classical filters when trained sufficiently. In exploring the deep learning denoising models focus was on unsupervised models i.e that do not require clean images for denoising. This was covered in detail in Chapter 2.

3.3.2 Preliminary Data Collection

Preliminary data was collected to familiarise ourselves with the LODOX® Statscan® system, given it was our first time working with the scanner. Additionally, this data helped in selecting appropriate phantoms to be used to train the ML models. This was through evaluating the performance of classical filters namely Non-Local Means (NLM),Block Matching and 3D filtering (BM3D) and Wavelet at default settings on the data using SNR and PSNR. Phantom images that most of the classical filters

Table 3.2: System Functional Requirements

ID	Requirement	Description	User Requirement
FR-01	Image Quality Enhancement	The model shall enhance SNR and PSNR to improve overall image clarity.	UR-01
FR-02	Anatomical Detail Preservation	The model shall optimise SSIM to ensure critical anatomical structures are preserved.	UR-02
FR-03	System Compatibility	The model shall integrate with DICOM-compliant medical imaging software, such as DVS® by LODOX®.	UR-03
FR-04	Efficient Processing	The model shall denoise a standard LODOX® Statscan® image within 5 seconds.	UR-04
FR-05	User Interface Design	The model shall provide a GUI for uploading, processing, and downloading images with minimal steps.	UR-05
FR-06	Scalability Features	The model shall support various input image resolutions and dimensions, adjusting algorithms accordingly.	UR-06
FR-07	Noise Level Adaptation	The model shall adaptively filter images with different noise levels to maintain high-quality output.	UR-07
FR-08	Artifact Minimisation	The model shall include techniques to detect and minimise artifacts introduced during the denoising process.	UR-08

struggled to denoise were then selected to be used for training. This ensured that only noise-rich phantom images could be used to train the Deep-learning models.

3.3.3 Model Selection and Preliminary Testing

Two critical factors guided the selection of the models to be used, i.e adaptability to learn to denoise across various noise types and not requiring clean images to learn denoising. Additionally, previous tests or applications of the models on medical image denoising or photon-limited image settings such as microscopy images was considered. The two models that met that criteria were N2N and N2V. They both use noisy image inputs to learn the denoising as was detailed in 2.3.3. Moreover, N2N had previously been tested on denoising Magnetic Resonance Imaging (MRI). Although MRI is predominantly affected by Rician noise, N2N is highly adaptable and can learn to denoise photon-limited images with sufficient training. In contrast, N2V was predominantly tested on microscopy images that are degraded by Poisson noise. Although, this is not the same condition as in LODOX® Statscan® given the high levels of Poisson noise, N2V is highly adaptable and has the potential to effectively denoise LODOX® Statscan® images.

These two models were then assessed using the preliminary data collected to understand how they perform and how various parameters can be adjusted further to enhance their performance on the LODOX® Statscan® images. This involved training them for 10 epochs with 10 iterations per epoch using only a single image for N2V and two images for N2N.

3.3.4 Data Collection

Phantom Types

Primarily, two classes of phantoms were used in this study, as discussed below:

1. **Medical Calibration Phantoms:** Used for Computed Tomography (CT) scans and bone density measurements. These phantoms are the clsest to human anatomy and are used to calibrate the LODOX® Statscan® system.
2. **Everyday Objects:** Include keyboards, calculators, metallic rulers, glass funnels, etc., used to model various noise scenarios and provide noise-rich images for model training.

Phantom Selection Criteria

The following criteria were used in selecting phantoms for scans:

1. **Affordability and availability:** only phantoms that were freely available to my supervisor and those provided by LODOX® were used. This meant that anatomical phantoms were not available.
2. **Artifacts Generation:** phantoms that were highly known to introduce artfiacts were used to deliberately introduce artifacts in the images so that the model could learn to remove such from the images.
3. **Presence of edges:** since most denoising models struggle with preserving edges, phantoms with nice and straight edges were also incorporated to aid in model training and test the trained model's ability to preserve edges, as this is a critical part of denoising.

Data Collection Procedure

Informed from findings from 3.3.4, new phantom scans of the noise-rich objects were scanned. This included the following phantoms scanned from various angles:

1. A Variety of tools available at the lab
2. Level
3. Keyboard
4. Computer Mouse
5. Calculator

6. Smartphone

The following scanning conditions were employed:

1. The scanning was done strictly during the day
2. The following parameters were set on the LODOX® Statscan® scanner for the scanning as detailed in Table 3.3 below:

Table 3.3: LODOX® Statscan® scanner configuration

Metric/Parameter	**Setting Used**
Procedure	Chest(lung) AP
Scan Time	0.00 ms
Exposure Time	66.00 ms
X-ray tube current	50.00 mA
X-ray Tube Voltage	120 kV(KVP)
Detector Binning	2
Scan Velocity	140 mm/s
Spatial Resolution	5.00 lp/mm

After the scans, all the processing done by the DVS® software by LODOX® was removed by unchecking the Lucid(R) and Denoise filters applied in the processing history menu, as shown in Figure 3.2 below. This ensured raw, unprocessed images were exported for model training.

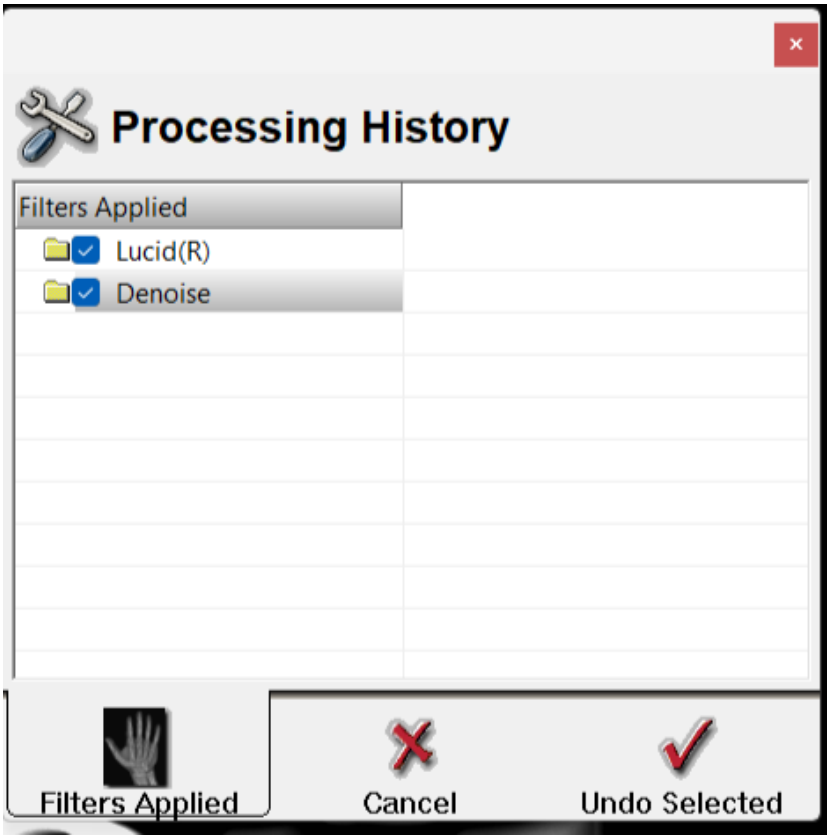

Figure 3.2: Illustration of unchecking the custom filters in the DVS® processing history menu

A total of 10 images were collected for training as shown in Figure 3.3 below:

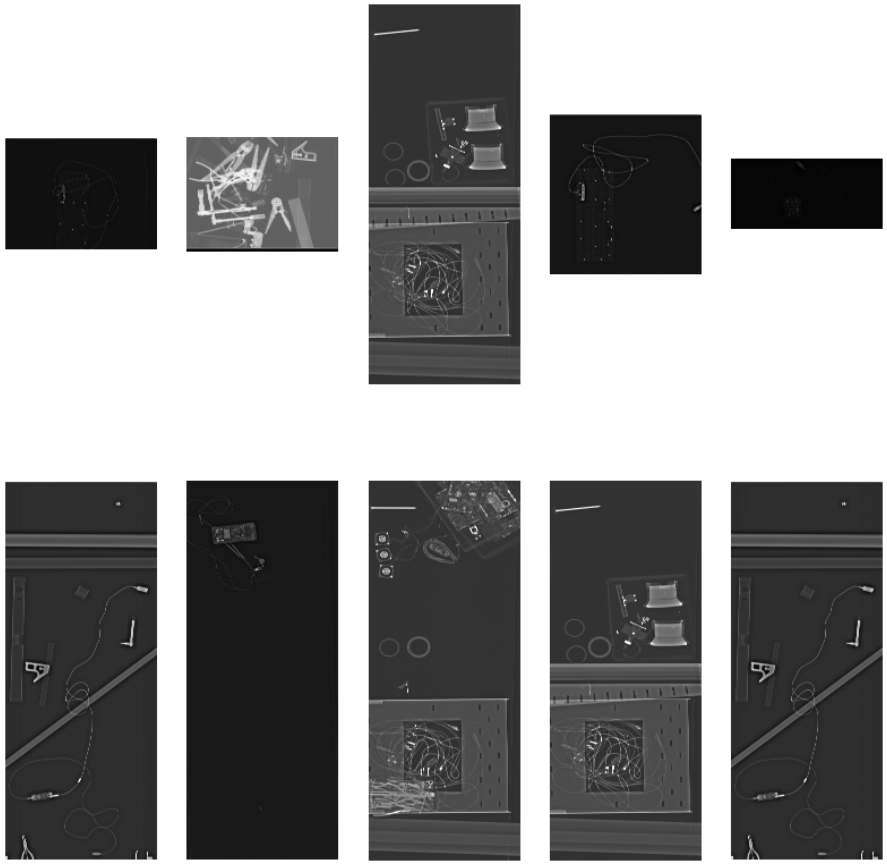

Figure 3.3: Set of training images collected

3.4 Deep Learning Models

The two models, N2N and N2V selected in section 3.3.3 above, are discussed below in terms of their theory and architecture. To understand these models effectively, a brief overview of traditional Convolutional Neural Networks (CNN)s is explored first to lay the groundwork required to understand the adaptions made to the N2N and N2V models.

3.4.1 Traditional CNN

Theory

Traditional CNNs learn to denoise images by mapping corrupted observations to clean versions. This is done through training a CNN with a large number of input and ground truth pairs(x_i, y_i) and then minimising the empirical risk as shown in Equation 3.1 below:

$$\arg\min_{\theta} \sum_{i} L\left(f_\theta(\hat{x}_i), y_i\right) \tag{3.1}$$

Where:

f_θ represents a parametric family of mappings (e.g., CNNs), under the loss function L.
$\hat{x}_i$ shows the corrupted input $\hat{x}_i \sim p(\hat{x}_i|y_i)$ is a random variable distributed according to the clean target.

This can be broken down further by treating each pixel prediction in output to have a specific receptive field $x_{RF}(i)$, i.e the set of input pixels influencing that output pixel prediction. Consequently, this shows that denoising can be achieved by extracting overlapping patches and feeding them to the network one by one, rendering the parametric mapping from equation 3.1to be rewritten as:

$$f(\mathbf{x}_{\mathrm{RF}(i)}; \theta) = \hat{y}_i \tag{3.2}$$

The training inputs are now seen as pairs$(\mathbf{x}^j_{\mathrm{RF}(i)}, \mathbf{y}^j_i)$ where $\mathbf{x}^j_{\mathrm{RF}(i)}$ is a patch around pixel i, extracted from the training input image and $\mathbf{y}^j_i$ is the corresponding target pixel value, extracted from the ground truth image at the same position. This now leads to the Equation 3.1 above to be refactored to Equation 3.3:

$$\arg\min_\theta \sum_j \sum_i L\left(f(\mathbf{x}^j_{\mathrm{RF}(i)}; \theta) = \hat{\mathbf{y}}^j_i, \mathbf{y}^j_i\right) \tag{3.3}$$

With an MSE Loss defined as:

$$L\left(\hat{\mathbf{y}}^j_i, \mathbf{y}^j_i\right) = \left(\hat{\mathbf{y}}^j_i - \mathbf{y}^j_i\right)^2 \tag{3.4}$$

Architecture

The CNN architecture that is of interest in our study is the U-Net architecture since both N2N and N2V modify this neural net type in their respective implementations. Additionally, it is widely used in medical image denoising because it can produce accurate segmentation even with small training datasets. A typical U-net generally consists of two key parts:

1. **Contracting path:** responsible for identifying relevant features in an image through using encoder layers to perform convolution operations to reduce the spatial resolution of feature maps whilst increasing their depth to capture abstract representations of the input.
2. **Expansive path:** Focuses on decoding the encoded data from the contracting path to locate the features whilst maintaining the input's spatial resolution. This is done through upsampling and performing convolutional operations.

An example of U-Net architecture is shown in Figure 3.4 below:

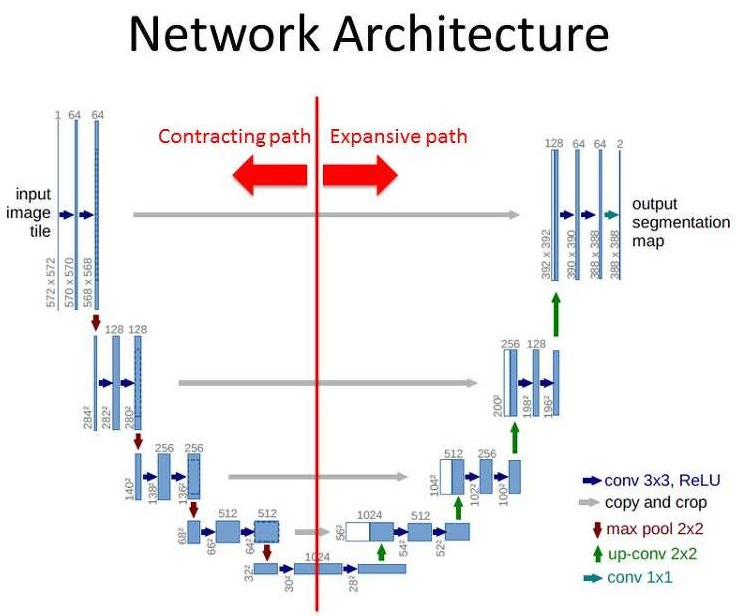

Figure 3.4: illustrates the U-Net architecture, which transforms a grayscale input image into a smaller binary segmentation map using a contracting-expansive path with skip connections and no padding, progressively reducing spatial dimensions while increasing feature depth.

3.4.2 N2N

Theory

N2N improves on the traditional CNN model by eliminating the dependency on input data on the equation 3.1 and using a trivial f_θ that outputs a learned scalar. This task reduces to a loss function, which can be viewed as an Machine Learning (ML) estimation by interpreting the loss function as the negative log-likelihood as shown in equation 3.5 below:

$$\arg\min_{\theta} \mathbb{E}_x \left\{ \mathbb{E}_{y|x} \left[L(f_\theta(x), y) \right] \right\} \tag{3.5}$$

From the above, it is deduced that the network can solve the point estimation problem separately for each input sample. Thus N2N works on the principle that the property of L2 minimisation that on expectation, the estimate remains unchanged when the targets are replaced with random numbers whose expectations match the targets. Consequently, the loss function holds under these conditions, and the optimal network parameters θ of Equation 3.5 also remain unchanged, if input-conditioned target distributions $p(y|x)$ are replaced with arbitrary distributions that have the same conditional expected values. As a consequence and factoring in the use of corrupted inputs the empirical minimisation task reduces to equation 3.6 below:

$$\arg\min_{\theta} \sum_{i} L\left(f_\theta(\hat{x}_i), \hat{y}_i\right) \tag{3.6}$$

With inputs being drawn from a corrupted distribution that is conditioned on the underlying, unobserved clean target y_i such that $E\{\hat{y}_i|\hat{x}_i\} = y_i$, given an infinite data, the solution is the same as that of equation 3.1 of traditional CNN.

N2N starts with a pair of noisy image pairs (x^j, $x^{j'}$), where

$$x^j = s^j + n^j \quad \text{and} \quad x^{j'} = s^{j'} + n^{j'} \tag{3.7}$$

The two training images are identical up to their noise components $n^j, n^{j'}$. Applying patch-based approach the training data is then viewed as pairs $\mathbf{x}^j_{\mathrm{RF}(i)}, \mathbf{x}_i{}'^j$, consisting of a noisy input patch $\mathbf{x}^j_{\mathrm{RF}(i)}$, extracted from x^j, and a noisy target, taken from x'^j at the position i. Similarly, to traditional CNN training, parameters are tuned to minimise the loss in equation 3.4, however, the only difference is that a noisy target is being used instead of ground truth data y_i.

Architecture

N2N architecture is a modified U-Net architecture consisting of the following three key parts:

1. **Contraction Part:** The contraction part consists of multiple Conv2D layers with 3x3 filters, typically using 64 filters to capture features from the input image. Optional dropout layers can be included to prevent overfitting by randomly zeroing a fraction of input units during training. Max-pooling layers with 2x2 filters are used to down-sample the feature maps, reducing spatial dimensions while retaining important features.

2. **Bottleneck Part:** In the bottleneck, two Conv2D layers with 3x3 filters further process the down-sampled feature maps. Optional dropout layers can be applied to prevent overfitting. Up-sampling with 2x2 layers increases the spatial dimensions, preparing the feature maps for the expansion phase.

3. **Expansion Part:** The expansion part includes Conv2D layers with 3x3 filters to refine the up-sampled feature maps and reconstruct the denoised image. Optional dropout layers help improve generalisation. 2x2 up-sampling layers restore the spatial dimensions of the feature maps to match the original input size.

The architecture of a sample N2N is visualised in Figure 3.5 below:

3.4.3 N2V

Theory

N2V is an extension of N2N in that it proposes that the two patches be extracted from a single image instead of two. It is based on the principle that upon extraction of a patch, the centre pixel can be masked and used as the target, allowing the network to learn to map the value at the centre of the

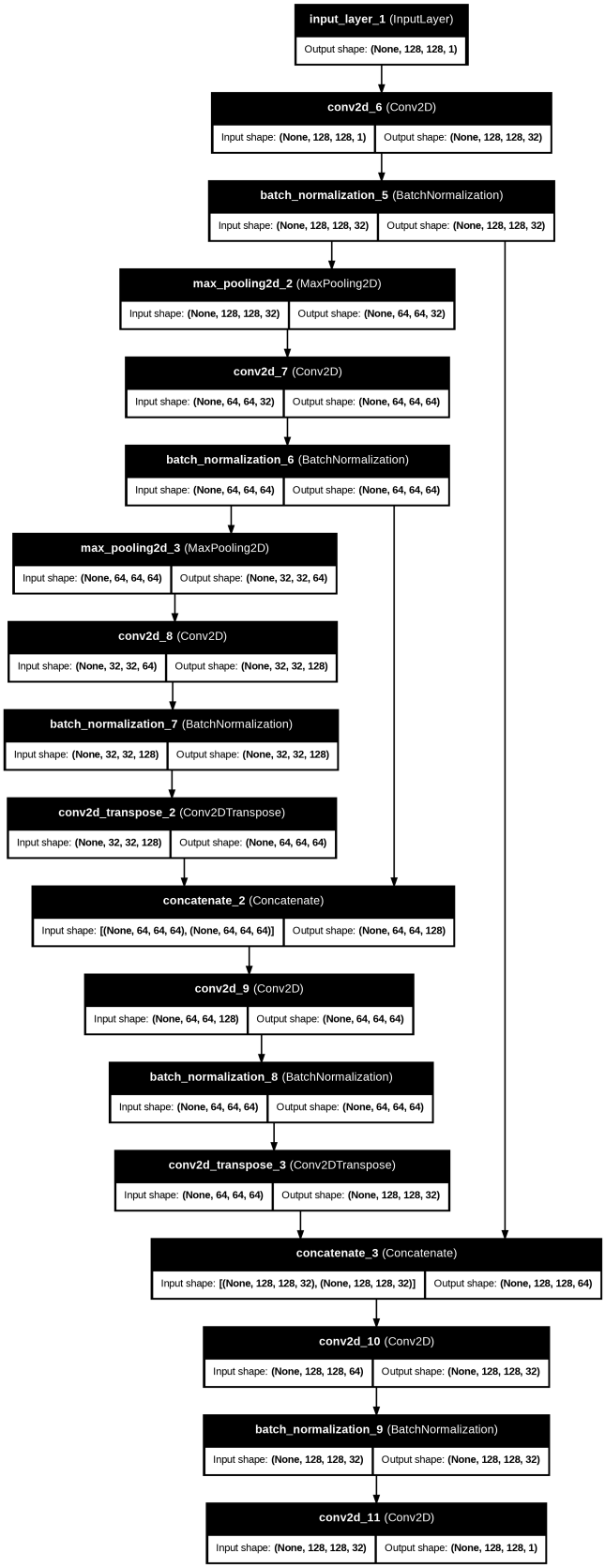

Figure 3.5: N2N architecture

input patch directly to the output.

To achieve this N2V has a set of assumptions:

1. Image generation is seen as $\mathbf{x} = \mathbf{s} + \mathbf{n}$ as a draw from the joint distribution $p(\mathbf{s}, \mathbf{n}) = p(\mathbf{s})p(\mathbf{n}|\mathbf{s})$
2. $p(\mathbf{s})$ is assumed to be an arbitrary distribution satisfying $p(\mathbf{s}_i|\mathbf{s}_j) \neq p(\mathbf{s}_i)$ for two pixels i and j within a certain radius of each other, with pixel $\mathbf{s}_i$ of the signal not statistically independent.
3. With respect to $\mathbf{n}$ a conditional distribution of the following form is assumed: $p(\mathbf{n}|\mathbf{s}) = \prod_i p(\mathbf{n}_i\mathbf{s}_i)$, indicating pixels values of the noise are conditionally independent given the signal.
4. Noise is assumed to be zero-mean i.e $\mathbb{E}[\mathbf{n}_i] = 0$ leading to $\mathbb{E}[\mathbf{x}_i] = \mathbf{s}_i$

Based on the above assumptions, it can be deduced that acquiring multiple images with the same underlying signal but different noise realisations, and then averaging them, will converge toward the true signal.

N2V uses a special receptive field with a blind spot at its centre, as shown in Figure 3.6 below; thus, CNN prediction $\hat{\mathbf{s}}_i$ for a pixel is affected by all input pixels in a square neighbourhood except for the input pixel $\mathbf{x}_i$ at its very location. This leads to less information than a traditional CNN; however, this is the advantage of the blindspot network i.e. its inability to learn identities. This is done by a masking scheme that replaces the value in the centre of each input patch with a randomly selected value from the surrounding area.

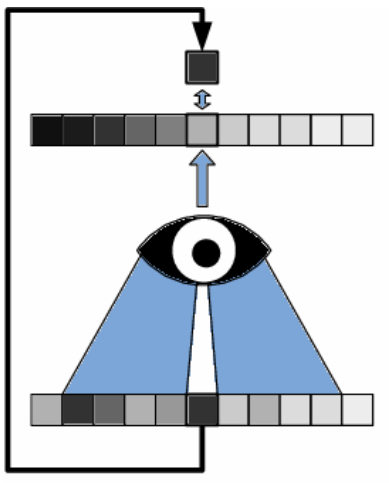

Figure 3.6: Blind-spot network showing the receptive field of a pixel, excluding the pixel itself.

The noise is assumed to be pixel-wise independent; thus, neighbouring pixels carry no information about the pixel, and therefore, it is impossible to produce an estimate that is better than a priori expected value(see 4). However, this is countered by the signal being assumed to contain statistical dependencies (see 2). As a result, the network can still estimate the signal $\mathbf{s}_i$ of a pixel by looking at its surroundings. Consequently, the blind network allows extraction of input patch and target value from the same noisy image. Thus the empirical risk becomes:

$$\arg\min_{\theta} \sum_{j} \sum_{i} L\left(f(\tilde{\mathbf{x}}^{j}_{\mathrm{RF}(i)}; \theta), \mathbf{x}^{j}_{i}\right) \tag{3.8}$$

The target $\mathbf{x}^{j}_{i}$ is equivalent to N2N's $\mathbf{x}^{`j}_{i}$ which is extracted from the second image. The two target values $\mathbf{x}^{j}_{i}$ and $\mathbf{x}^{`j}_{i}$ have an equal signal $\mathbf{s}^{j}_{i}$with noise components being two independent samples from the same distribution $p(\mathbf{n}_i|\mathbf{s}_j)$. This, in principle, shows that using a blindspot network, an individual noisy image can be used to train the model.

Architecture

N2V is based on a modified U-Net architecture and consists of three main sections:

1. **Contraction Part**: Multiple Conv2D layers with 3x3 filters (typically 64 filters each) capture features from the input image. Optional dropout layers prevent overfitting, and 2x2 max-pooling layers down-sample the feature maps, reducing spatial dimensions while retaining important features.

2. **Bottleneck Part**: Two Conv2D layers with 3x3 filters further process the down-sampled feature maps. Optional dropout layers are included, and 2x2 up-sampling layers increase the spatial dimensions of the feature maps, preparing them for the expansion part.

3. **Expansion Part**: Multiple Conv2D layers with 3x3 filters refine the up-sampled feature maps and reconstruct the denoised image. Optional dropout layers enhance generalisation, and 2x2 up-sampling layers restore the feature maps to the original input size.

A visual representation of the architecture is shown in Figure 3.7 below:

3.5 Research Instruments

3.5.1 Software

The software was crucial for two parts of the process. First, software was needed to interface with the LODOX® Statscan® scanner to collect data. The software used to interface with the scanner was the DVS® by LODOX® Systems Pty Limited. It was also used to get the raw image and export it into DICOM file format for denoising in other software platforms.

Secondly, software was needed to develop the denoising model.The choice of programming language to develop the denoising model is critical to ensure the model is effectively implemented, scalable, and maintainable while providing access to necessary libraries and tools for medical image processing. Per the user requirements outlined in section 3.2 above, the following programming languages were considered: Python and MATLAB®. The criteria for choosing a programming language for implementation were :

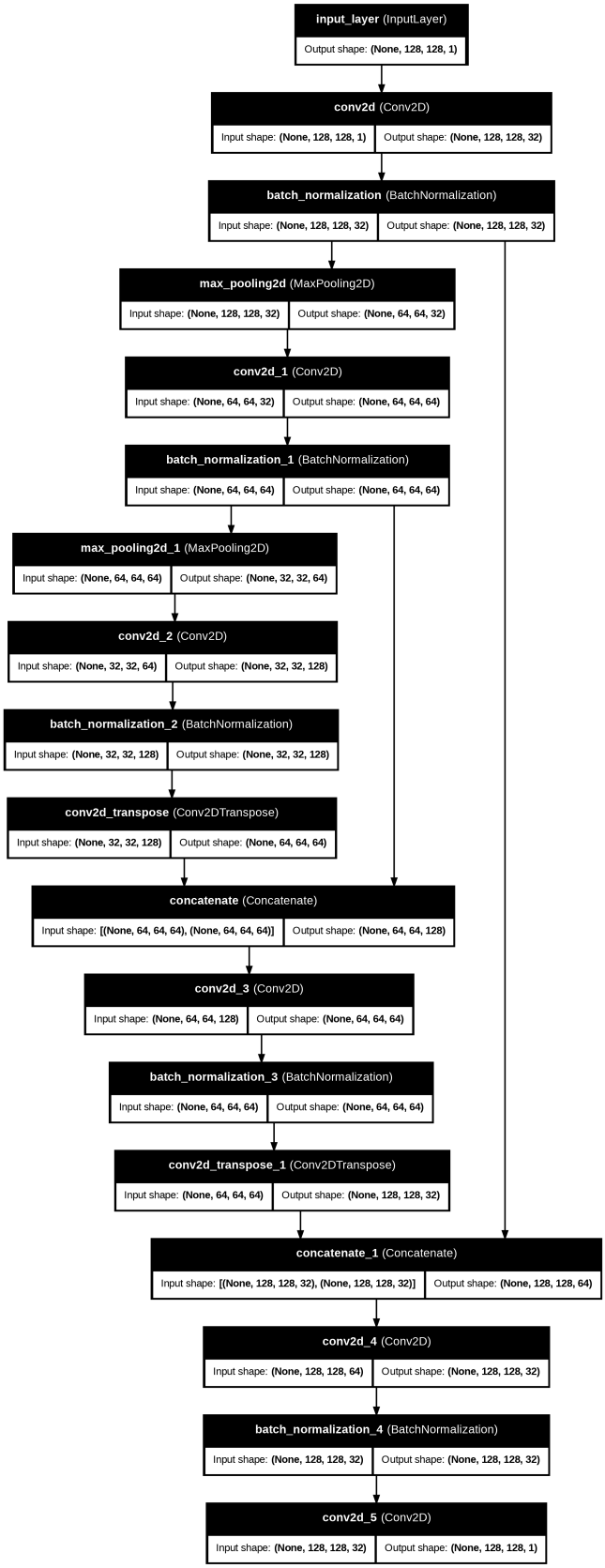

Figure 3.7: N2V architecture

- Ease of development

- Community support
- Integration with deep learning frameworks
- DICOM Support
- Integration and Interoperability

A detailed comparison is shown in Table 3.4 below:

Table 3.4: Comparison of Python and MATLAB®

Criteria	**Python**	**MATLAB®**
Deep Learning Frameworks	Extensive library support for deep learning (TensorFlow, PyTorch, Keras)	Built-in tools for image processing and analysis (Deep Learning Toolbox, Image Processing Toolbox).
DICOM Support	Strong support for medical imaging (pydicom, SimpleITK)	Robust support for DICOM and medical image processing.
Community support	A large, active community with vast resources makes finding help and solutions easier.	Strong academic support but a smaller community compared to Python for deep learning.
Ease of development	Fast prototyping with a vast array of pre-built models and functions available.	Very efficient for initial development and testing with built-in functions for common tasks.
Integration and Interoperability	Integrates well with other software and tools, making it highly flexible.	Excellent integration with hardware and other MathWorks products.

Python is chosen as the primary programming language for implementing the two denoising model due to its extensive library support, ease of use, and strong community resources as depicted in Table 3.4 above.

3.5.2 Hardware

The LODOX® Statscan® scanner model was used to do the scans. It is housed at the Medical Imaging Lab, UCT HUB, Division of Biomedical Engineering. The other hardware used were the phantoms that were being scanned to provide images for model training, validation and testing as was detailed in section 3.3.4.

3.6 Performance metrics

The following groups of performance metrics were used to measure the performance metrics: Proxy quantitative, qualitative, and no-reference quality and are discussed in detail below:

3.6.1 Proxy Quantitative Analysis

Traditional metrics like SNR, PSNR and SSIM cannot be used directly as there is no access to clean images; thus, proxy versions of these metrics were used by treating the denoised image as a proxy for the clean image and comparing it with the original noisy input. This will give relative noise performance. These proxy measurements are discussed in Table 3.5 below:

Table 3.5: Proxy Quantitative Analysis

Metric	Importance
pseudo-SNR	Quantifies the noise level relative to image signal with higher SNR values indicating beer noise suppression
pseudo-PSNR	Measures the peak error between the original and denoised images, with higher values indicating better performance.
pseudo-SSIM	Evaluates the similarity between the original and denoised images based on luminance, contrast, and structure. It is vital to ensure that the structural integrity of LODOX® Statscan® images is maintained.
Noise Residual Analysis	Analyses the difference between the noisy input and denoised output to assess the efficacy of the model in denoising the image.

3.6.2 Qualitative Metrics

Drawing from [3] quality analysis, the denoised images were visually compared against the processed output from the DVS® software using an eye test to assess image quality. Additionally, the denoised images were compared to their noisy counterparts to evaluate differences in clarity, contrast, and overall usability. This visual assessment helps to identify improvements in image quality and ensures that the denoising process enhances the diagnostic value of the images without introducing artifacts or losing critical information.

3.6.3 No-Reference Quality Metrics

The following no-reference metrics were used to evaluate the image quality since they were inherently designed to assess image quality without needing a clean reference image. The following no-reference metrics were used:

- Natural Image Quality Evaluator (NIQE): This model evaluates image quality by measuring deviations from statistical regularities found in natural images.
- Blind/Referenceless Image Spatial Quality Evaluator (BRISQUE): calculates quality using features that capture natural scene statistics.
- Perception-based Image Quality Evaluator (PIQE): computes image quality based on perceptual information in localised spatial regions of the image.

3.7 Limitations

1. **Use of Non-Anatomical Phantoms**: The study utilizes non-clinical phantoms that do not accurately model human tissue. This limitation may hinder the direct application of findings to clinical settings, as the phantoms lack the anatomical complexities present in actual human subjects, potentially impacting the generalisability of the results.
2. **Time Constraints on Model Training**: The machine learning models were trained within the confines of a 12-week project duration. Extended training time could have improved the efficacy and performance of these models. The limited training period may not have allowed the models to be fully optimised, potentially affecting the robustness of the denoising outcomes.
3. **Limited Scope of Unsupervised Models**: The methodology considers only two unsupervised denoising models. While there is potential for better performance with additional models, the study is constrained by the availability and maturity of unsupervised techniques. As discussed in Chapter 2, most advanced denoising models currently rely on supervised learning, which limits the exploration of a broader range of unsupervised approaches.

These limitations highlight areas where the methodology could be refined in future studies, such as the inclusion of more realistic phantoms, extended training periods, and the exploration of a wider variety of unsupervised denoising models.

3.8 Ethics

Ethics was complied with as set out and specified by the UCT Ethics guideline and guidelines stipulated by the EBE faculty. No human subjects are used in the research, and the use of Artificial Intelligence in this research qualifies as minimal risk. A detailed Ethics approval and application form is detailed in Appendix B.

3.9 Conclusion

In conclusion, this chapter provided a comprehensive overview of the research methodology employed in developing the denoising model for LODOX® Statscan®images. The research design was carefully structured, beginning with exploring relevant literature and progressing through preliminary data collection, model selection, and the rigorous testing and validation of the chosen models. The methodology emphasised the importance of selecting appropriate phantoms and utilising both classical and advanced deep learning techniques to achieve the desired denoising outcomes. The software and hardware tools were carefully chosen to ensure compatibility and efficiency, with Python emerging as the preferred language due to its extensive library support and scalability in machine learning tasks.

The analysis phase utilised a combination of quantitative metrics, such as SNR, PSNR, and SSIM, alongside qualitative assessments to validate the effectiveness of the denoising models. Despite the limitations of using non-anatomical phantoms and the constrained training period, the study successfully demonstrated the potential of unsupervised deep learning models, particularly N2N and N2V, in enhancing the quality of LODOX® Statscan®images.

Chapter 4

Design

Chapter 5

Results

Chapter 6

Conclusions

Bibliography

[1] C.-Y. Fu, S.-C. Wu, and R.-J. Chen, "Lodox/Statscan provides rapid identification of bullets in multiple gunshot wounds," *The American Journal of Emergency Medicine*, vol. 26, no. 8, pp. 965.e5–965.e7, Oct. 2008. [Online]. Available: https://www.sciencedirect.com/science/article/pii/S0735675708001265

[2] C.-Y. Fu, Y.-C. Wang, C.-H. Hsieh, and R.-J. Chen, "Lodox/Statscan provides benefits in evaluation of gunshot injuries," *The American Journal of Emergency Medicine*, vol. 29, no. 7, pp. 823–827, Sep. 2011. [Online]. Available: https://www.sciencedirect.com/science/article/pii/S0735675711001331

[3] M. Juneja, J. S. Minhas, N. Singla, R. Kaur, and P. Jindal, "Denoising techniques for cephalometric x-ray images: A comprehensive review," *Multimedia Tools and Applications*, vol. 83, no. 17, pp. 49 953–49 991, May 2024. [Online]. Available: https://doi.org/10.1007/s11042-023-17495-z

[4] S. Beningfield, H. Potgieter, A. Nicol, S. van As, G. Bowie, E. Hering, and E. Lätti, "Report on a new type of trauma full-body digital X-ray machine," *Emergency Radiology*, vol. 10, no. 1, pp. 23–29, Apr. 2003. [Online]. Available: https://doi.org/10.1007/s10140-003-0271-x

[5] B. Amirlak, B. Zakhary, K. Weichman, H. Ahluwalia, A. R. Forse, and R. D. Gaines, "Novel use of Lodox® Statscan® in a level one trauma center," *Ulus Travma Acil Cerrahi Derg*, vol. 15, no. 6, 2009.

[6] "Full-body radiography (LODOX Statscan) in trauma and emergency medicine: a report from the first European installation site." [Online]. Available: https://journals.sagepub.com/doi/epdf/10.1177/1460408610382493

[7] A. K. Exadaktylos, L. M. Benneker, V. Jeger, L. Martinolli, H. M. Bonel, S. Eggli, H. Potgieter, and H. Zimmermann, "Total-body digital X-ray in trauma: An experience report on the first operational full body scanner in Europe and its possible role in ATLS," *Injury*, vol. 39, no. 5, pp. 525–529, May 2008. [Online]. Available: https://www.sciencedirect.com/science/article/pii/S0020138307004275

[8] Lodox Systems, "Lodox solution for trauma units," August 2018, accessed: August 8, 2024. [Online Video]. Available: https://www.youtube.com/watch?v=M6gmVEs5wMs.

[9] S. P. Whiley, H. Alves, and S. Grace, "Full-Body X-Ray Imaging to Facilitate Triage: A Potential Aid in High-Volume Emergency Departments," *Emergency Medicine International*, vol. 2013, no. 1, p. 437078, 2013, _eprint: https://onlinelibrary.wiley.com/doi/pdf/10.1155/2013/437078. [Online]. Available: https://onlinelibrary.wiley.com/doi/abs/10.1155/2013/437078

[10] M. D. Villiers, "Limited angle tomography," Ph.D. dissertation, Dept. Elect. Eng., Univ. of Cape Town, Cape Town, South Africa, June 2004, [Online]. Available: http://www.dip.ee.uct.ac.za/publications/theses/PhDMattieu.pdf.

[11] D. Y. Martin, "Project brief," https://amathuba.uct.ac.za, (Accessed on 10/20/2024).

[12] N. R. Huber, A. Ferrero, K. Rajendran, F. Baffour, K. N. Glazebrook, F. E. Diehn, A. Inoue, J. G. Fletcher, L. Yu, S. Leng, and C. H. McCollough, "Dedicated convolutional neural network for noise reduction in ultra-high-resolution photon-counting detector computed tomography," *Physics in Medicine & Biology*, vol. 67, no. 17, p. 175014, Sep. 2022, publisher: IOP Publishing. [Online]. Available: https://dx.doi.org/10.1088/1361-6560/ac8866

[13] D. S. Evangelopoulos, S. Deyle, H. Zimmermann, and A. K. Exadaktylos, "Personal experience with whole-body, low-dosage, digital X-ray scanning (LODOX-Statscan) in trauma," *Scandinavian Journal of Trauma, Resuscitation and Emergency Medicine*, vol. 17, no. 1, p. 41, Sep. 2009. [Online]. Available: https://doi.org/10.1186/1757-7241-17-41

[14] A. P. Harrison, Z. Xu, A. Pourmorteza, D. A. Bluemke, and D. J. Mollura, "A multichannel block-matching denoising algorithm for spectral photon-counting CT images," *Medical Physics*, vol. 44, no. 6, pp. 2447–2452, 2017, _eprint: https://onlinelibrary.wiley.com/doi/pdf/10.1002/mp.12225. [Online]. Available: https://onlinelibrary.wiley.com/doi/abs/10.1002/mp.12225

[15] M. A. Haidekker, "Introduction," in *Medical Imaging Technology*, M. A. Haidekker, Ed. New York, NY: Springer, 2013, pp. 1–12. [Online]. Available: https://doi.org/10.1007/978-1-4614-7073-1_1

[16] ——, "X-Ray Projection Imaging," in *Medical Imaging Technology*, M. A. Haidekker, Ed. New York, NY: Springer, 2013, pp. 13–35. [Online]. Available: https://doi.org/10.1007/978-1-4614-7073-1_2

[17] ——, "Trends in Medical Imaging Technology," in *Medical Imaging Technology*, M. A. Haidekker, Ed. New York, NY: Springer, 2013, pp. 111–119. [Online]. Available: https://doi.org/10.1007/978-1-4614-7073-1_7

[18] W. J. H. Veldkamp, L. J. M. Kroft, and J. Geleijns, "Dose and perceived image quality in chest radiography," *European Journal of Radiology*, vol. 72, no. 2, pp. 209–217, Nov. 2009. [Online]. Available: https://www.sciencedirect.com/science/article/pii/S0720048X09003349

[19] S. Lahmiri, "An iterative denoising system based on Wiener filtering with application to biomedical images," *Optics & Laser Technology*, vol. 90, pp. 128–132, May 2017. [Online]. Available: https://www.sciencedirect.com/science/article/pii/S0030399216304480

[20] J. A. Seibert, "Tradeoffs between image quality and dose," *Pediatric Radiology*, vol. 34, no. 3, pp. S183–S195, Oct. 2004. [Online]. Available: https://doi.org/10.1007/s00247-004-1268-7

[21] "Noise Characteristic and its Removal in digital Radiographic System." [Online]. Available: https://www.ndt.net/article/wcndt00/papers/idn375/idn375.htm

[22] W. Huda and R. B. Abrahams, "Radiographic Techniques, Contrast, and Noise in X-Ray Imaging," *American Journal of Roentgenology*, vol. 204, no. 2, pp. W126–W131, Feb. 2015, publisher: American Roentgen Ray Society. [Online]. Available: https://ajronline.org/doi/full/10.2214/AJR.14.13116

[23] D. S. Kim, "Measurements of the noise power spectrum for digital x-ray imaging devices," *Physics in Medicine & Biology*, vol. 69, no. 3, p. 03TR01, Jan. 2024, publisher: IOP Publishing. [Online]. Available: https://dx.doi.org/10.1088/1361-6560/ad1999

[24] E. N. Manson, V. A. Ampoh, E. Fiagbedzi, J. H. Amuasi, J. J. Flether, and C. Schandorf, "Image Noise in Radiography and Tomography: Causes, Effects and Reduction Techniques," *Current Trends in Clinical & Medical Imaging*, vol. 3, no. 4, pp. 86–91, Oct. 2019, publisher: Juniper Publishers. [Online]. Available: http://juniperpublishers.com/ctcmi/CTCMI.MS.ID.555620.php

[25] T. B. Chandra and K. Verma, "Analysis of quantum noise-reducing filters on chest X-ray images: A review," *Measurement*, vol. 153, p. 107426, Mar. 2020. [Online]. Available: https://www.sciencedirect.com/science/article/pii/S026322411931293X

[26] K. B. Khan, A. A. Khaliq, M. Shahid, and J. A. Shah, "A new approach of weighted gradient filter for denoising of medical images in the presence of Poisson noise," *Tehnički vjesnik*, vol. 23, no. 6, pp. 1755–1762, Nov. 2016, publisher: Sveučilište u Slavonskom Brodu, Stojarski fakultet. [Online]. Available: https://hrcak.srce.hr/clanak/249928

[27] D. Thanh, P. Surya, and L. M. Hieu, "A Review on CT and X-Ray Images Denoising Methods," *Informatica*, vol. 43, no. 2, Jun. 2019, number: 2. [Online]. Available: https://www.informatica.si/index.php/informatica/article/view/2179

[28] P. Gravel, G. Beaudoin, and J. De Guise, "A method for modeling noise in medical images," *IEEE Transactions on Medical Imaging*, vol. 23, no. 10, pp. 1221–1232, Oct.

2004, conference Name: IEEE Transactions on Medical Imaging. [Online]. Available: https://ieeexplore.ieee.org/abstract/document/1339429

[29] B. Goyal, A. Dogra, S. Agrawal, and B. S. Sohi, "Noise Issues Prevailing in Various Types of Medical Images," *Biomedical and Pharmacology Journal*, vol. 11, no. 3, pp. 1227–1237, Sep. 2018. [Online]. Available: https://biomedpharmajournal.org/vol11no3/noise-issues-prevailing-in-various-types-of-medical-images/

[30] M. Warner, "Understanding and Managing Noise Sources in X-ray Imaging," Apr. 2020. [Online]. Available: https://www.carestream.com/blog/2020/04/21/understanding-and-managing-noise-sources-in-x-ray-imaging/

[31] N. Umadevi and D. S. N. Geethalakshmi, "IMPROVED HYBRID MODEL FOR DENOISING POISSON CORRUPTED X-RAY IMAGES," vol. 3, no. 7, 2011.

[32] H. Dong, L. Zhao, Y. Shu, and N. N. Xiong, "X-ray image denoising based on wavelet transform and median filter," *Applied Mathematics and Nonlinear Sciences*, vol. 5, no. 2, pp. 435–442, Jul. 2020. [Online]. Available: https://sciendo.com/article/10.2478/amns.2020.2.00062

[33] N. Kumar and M. Nachamai, "Noise Removal and Filtering Techniques used in Medical Images," *Oriental journal of computer science and technology*, vol. 10, no. 1, pp. 103–113, Mar. 2017. [Online]. Available: http://www.computerscijournal.org/vol10no1/noise-removal-and-filtering-techniques-used-in-medical-images/

[34] S. Lee and Y. Lee, "The impact of improved non-local means denoising algorithm on photon-counting X-ray images using various Al additive filtrations," *Nuclear Instruments and Methods in Physics Research Section A: Accelerators, Spectrometers, Detectors and Associated Equipment*, vol. 1027, p. 166244, Mar. 2022. [Online]. Available: https://www.sciencedirect.com/science/article/pii/S0168900221010846

[35] T. Kirti, K. Jitendra, and S. Ashok, "Poisson noise reduction from X-ray images by region classification and response median filtering," *Sādhanā*, vol. 42, no. 6, pp. 855–863, Jun. 2017. [Online]. Available: https://doi.org/10.1007/s12046-017-0654-4

[36] D. Kipele and K. Greyson, "Poisson Noise Reduction with Nonlocal-PCA Hybrid Model in Medical X-ray Images," *Journal of Image and Graphics*, pp. 178–184, Jun. 2023.

[37] I. Mandić, H. Peić, J. Lerga, and I. Štajduhar, "Denoising of X-ray Images Using the Adaptive Algorithm Based on the LPA-RICI Algorithm," *Journal of Imaging*, vol. 4, no. 2, p. 34, Feb. 2018, number: 2 Publisher: Multidisciplinary Digital Publishing Institute. [Online]. Available: https://www.mdpi.com/2313-433X/4/2/34

[38] K. V. Thakur, O. H. Damodare, and A. M. Sapkal, "Poisson Noise Reducing Bilateral Filter," *Procedia Computer Science*, vol. 79, pp. 861–865, Jan. 2016. [Online]. Available: https://www.sciencedirect.com/science/article/pii/S1877050916002180

[39] L. I. Rudin, S. Osher, and E. Fatemi, "Nonlinear total variation based noise removal algorithms," *Physica D: Nonlinear Phenomena*, vol. 60, no. 1, pp. 259–268, Nov. 1992. [Online]. Available: https://www.sciencedirect.com/science/article/pii/016727899290242F

[40] I. Rodrigues, J. Sanches, and J. Bioucas-Dias, "Denoising of medical images corrupted by Poisson noise," in *2008 15th IEEE International Conference on Image Processing*, Oct. 2008, pp. 1756–1759, iSSN: 2381-8549. [Online]. Available: https://ieeexplore.ieee.org/abstract/document/4712115

[41] Y. Lee, "X-ray image denoising with fast non-local means (FNLM) approach using acceleration function in CdTe semiconductor photon counting detector (PCD): Monte Carlo simulation study," *Optik*, vol. 172, pp. 456–461, Nov. 2018. [Online]. Available: https://www.sciencedirect.com/science/article/pii/S0030402618310234

[42] N. Dey, L. Blanc-Feraud, C. Zimmer, Z. Kam, J.-C. Olivo-Marin, and J. Zerubia, "A deconvolution method for confocal microscopy with total variation regularization," in *2004 2nd IEEE International Symposium on Biomedical Imaging: Nano to Macro (IEEE Cat No. 04EX821)*, Apr. 2004, pp. 1223–1226 Vol. 2. [Online]. Available: https://ieeexplore.ieee.org/abstract/document/1398765

[43] T. Le, R. Chartrand, and T. J. Asaki, "A Variational Approach to Reconstructing Images Corrupted by Poisson Noise," *Journal of Mathematical Imaging and Vision*, vol. 27, no. 3, pp. 257–263, Apr. 2007. [Online]. Available: https://doi.org/10.1007/s10851-007-0652-y

[44] V. B. S. Prasath, "Quantum Noise Removal in X-Ray Images with Adaptive Total Variation Regularization," *Informatica*, vol. 28, no. 3, pp. 505–515, Jan. 2017, publisher: Vilnius University Institute of Data Science and Digital Technologies. [Online]. Available: https://informatica.vu.lt/journal/INFORMATICA/article/859

[45] H. Liu, Z. Zhang, L. Xiao, and Z. Wei, "Poisson noise removal based on nonlocal total variation with Euler's elastica pre-processing," *Journal of Shanghai Jiaotong University (Science)*, vol. 22, no. 5, pp. 609–614, Oct. 2017. [Online]. Available: https://doi.org/10.1007/s12204-017-1878-5

[46] M. Mahmoudi and G. Sapiro, "Fast image and video denoising via nonlocal means of similar neighborhoods," *IEEE Signal Processing Letters*, vol. 12, no. 12, pp. 839–842, 2005.

[47] P. Coupé, P. Yger, and C. Barillot, "Fast Non Local Means Denoising for 3D MR Images," in *Medical Image Computing and Computer-Assisted Intervention – MICCAI 2006*, R. Larsen, M. Nielsen, and J. Sporring, Eds. Berlin, Heidelberg: Springer, 2006, pp. 33–40.

[48] C.-A. Deledalle, F. Tupin, and L. Denis, "Poisson nl means: Unsupervised non local means for poisson noise," in *2010 IEEE International Conference on Image Processing*, 2010, pp. 801–804.

[49] J. Shim, M. Yoon, and Y. Lee, "Feasibility of newly designed fast non local means (FNLM)-based noise reduction filter for X-ray imaging: A simulation study," *Optik*, vol. 160, pp. 124–130, May 2018. [Online]. Available: https://www.sciencedirect.com/science/article/pii/S0030402618301207

[50] "The Wiener filter." [Online]. Available: https://homepages.inf.ed.ac.uk/rbf/CVonline/LOCAL_COPIES/VELDHUIZEN/node15.html

[51] L. Wang, J. Lu, Y. Li, T. Yahagi, and T. Okamoto, "Noise removal for medical X-ray images in wavelet domain," *Electrical Engineering in Japan*, vol. 163, no. 3, pp. 37–46, 2008, _eprint: https://onlinelibrary.wiley.com/doi/pdf/10.1002/eej.20486. [Online]. Available: https://onlinelibrary.wiley.com/doi/abs/10.1002/eej.20486

[52] V. Göreke, "A novel method based on Wiener filter for denoising Poisson noise from medical X-Ray images," *Biomedical Signal Processing and Control*, vol. 79, p. 104031, Jan. 2023. [Online]. Available: https://www.sciencedirect.com/science/article/pii/S1746809422005080

[53] F. Luisier, C. Vonesch, T. Blu, and M. Unser, "Fast interscale wavelet denoising of poisson-corrupted images," *Signal Processing*, vol. 90, no. 2, pp. 415–427, 2010. [Online]. Available: https://www.sciencedirect.com/science/article/pii/S0165168409003016

[54] K. Timmermann and R. Nowak, "Multiscale modeling and estimation of poisson processes with application to photon-limited imaging," *IEEE Transactions on Information Theory*, vol. 45, no. 3, pp. 846–862, 1999.

[55] B. Zhang, J. M. Fadili, and J.-L. Starck, "Wavelets, ridgelets, and curvelets for poisson noise removal," *IEEE Transactions on Image Processing*, vol. 17, no. 7, pp. 1093–1108, 2008.

[56] S. Gupta, L. Kaur, R. Chauhan, and S. Saxena, "A wavelet based statistical approach for speckle reduction in medical ultrasound images," in *TENCON 2003. Conference on Convergent Technologies for Asia-Pacific Region*, vol. 2, 2003, pp. 534–537 Vol.2.

[57] L. Du, Y. Wen, and J. Ma, "Dual tree complex wavelet transform and bayesian estimation based denoising of poission-corrupted x-ray images," in *2013 Fourth International Conference on Intelligent Control and Information Processing (ICICIP)*, 2013, pp. 598–603.

[58] M. Makitalo and A. Foi, "Optimal inversion of the generalized anscombe transformation for poisson-gaussian noise," *IEEE Transactions on Image Processing*, vol. 22, no. 1, pp. 91–103, 2013.

[59] J. Ren, A. Cai, N. Liang, Y. Wang, X. Zhang, L. Li, and B. Yan, "A simulation study on photon-counting denoising based on subspace decomposition," in

5th International Conference on Information Science, Electrical, and Automation Engineering (ISEAE 2023), vol. 12748. SPIE, Aug. 2023, pp. 80–86. [Online]. Available: https://www.spiedigitallibrary.org/conference-proceedings-of-spie/12748/127480E/A-simulation-study-on-photon-counting-denoising-based-on-subspace/10.1117/12.2689447.full

[60] J. Salmon, Z. Harmany, C.-A. Deledalle, and R. Willett, "Poisson noise reduction with non-local pca," *Journal of mathematical imaging and vision*, vol. 48, pp. 279–294, 2014.

[61] W. Feng, H. Qiao, and Y. Chen, "Poisson noise reduction with higher-order natural image prior model," *SIAM Journal on Imaging Sciences*, vol. 9, no. 3, pp. 1502–1524, 2016. [Online]. Available: https://doi.org/10.1137/16M1072930

[62] J. Jisha and V. Sureshkumar, "Poisson noise removal in biomedical images using non-linear techniques," *International Journal of Advanced Research in Electrical, Electronics and Instrumentation Engineering*, vol. 3, pp. 131–136, 2014.

[63] K. Dabov, A. Foi, V. Katkovnik, and K. Egiazarian, "Image denoising by sparse 3-d transform-domain collaborative filtering," *IEEE Transactions on Image Processing*, vol. 16, no. 8, pp. 2080–2095, 2007.

[64] K. He, J. Sun, and X. Tang, "Guided image filtering," *IEEE Transactions on Pattern Analysis and Machine Intelligence*, vol. 35, no. 6, pp. 1397–1409, 2013.

[65] G. Treece, "The bitonic filter: Linear filtering in an edge-preserving morphological framework," *IEEE Transactions on Image Processing*, vol. 25, no. 11, pp. 5199–5211, 2016.

[66] S. G. Hariharan, C. Kaethner, N. Strobel, M. Kowarschik, S. Albarqouni, R. Fahrig, and N. Navab, "Learning-Based X-Ray Image Denoising Utilizing Model-Based Image Simulations," in *Medical Image Computing and Computer Assisted Intervention – MICCAI 2019*, D. Shen, T. Liu, T. M. Peters, L. H. Staib, C. Essert, S. Zhou, P.-T. Yap, and A. Khan, Eds. Cham: Springer International Publishing, 2019, pp. 549–557.

[67] R. Nadkarni, D. P. Clark, A. J. Allphin, and C. T. Badea, "A Deep Learning Approach for Rapid and Generalizable Denoising of Photon-Counting Micro-CT Images," *Tomography*, vol. 9, no. 4, pp. 1286–1302, Aug. 2023, number: 4 Publisher: Multidisciplinary Digital Publishing Institute. [Online]. Available: https://www.mdpi.com/2379-139X/9/4/102

[68] J. Lehtinen, J. Munkberg, J. Hasselgren, S. Laine, T. Karras, M. Aittala, and T. Aila, "Noise2Noise: Learning image restoration without clean data," in *Proceedings of the 35th International Conference on Machine Learning*, ser. Proceedings of Machine Learning Research, J. Dy and A. Krause, Eds., vol. 80. PMLR, 10–15 Jul 2018, pp. 2965–2974. [Online]. Available: https://proceedings.mlr.press/v80/lehtinen18a.html

[69] S. Wang, Z. Su, L. Ying, X. Peng, S. Zhu, F. Liang, D. Feng, and D. Liang, "Accelerating magnetic resonance imaging via deep learning," in *2016 IEEE 13th international symposium on biomedical imaging (ISBI)*. IEEE, 2016, pp. 514–517.

[70] D. Lee, J. Yoo, and J. C. Ye, "Deep residual learning for compressed sensing mri," in *2017 IEEE 14th International Symposium on Biomedical Imaging (ISBI 2017)*, 2017, pp. 15–18.

[71] A. Krull, T.-O. Buchholz, and F. Jug, "Noise2void - learning denoising from single noisy images," in *2019 IEEE/CVF Conference on Computer Vision and Pattern Recognition (CVPR)*, 2019, pp. 2124–2132.

[72] K. Zhang, W. Zuo, Y. Chen, D. Meng, and L. Zhang, "Beyond a gaussian denoiser: Residual learning of deep cnn for image denoising," *IEEE Transactions on Image Processing*, vol. 26, no. 7, pp. 3142–3155, 2017.

[73] S. Chang, J. F. M. Jr, E. K. Koons, H. Gong, C. H. McCollough, and S. Leng, "Improved noise reduction in photon-counting detector CT using prior knowledge-aware iterative denoising neural network," *Journal of Medical Imaging*, vol. 11, no. S1, p. S12804, May 2024, publisher: SPIE. [Online]. Available: https://www.spiedigitallibrary.org/journals/journal-of-medical-imaging/volume-11/issue-S1/S12804/Improved-noise-reduction-in-photon-counting-detector-CT-using-prior/10.1117/1.JMI.11.S1.S12804.full

[74] F. I. Baffour, N. R. Huber, A. Ferrero, K. Rajendran, K. N. Glazebrook, N. B. Larson, S. Kumar, J. M. Cook, S. Leng, E. R. Shanblatt, C. H. McCollough, and J. G. Fletcher, "Photon-counting Detector CT with Deep Learning Noise Reduction to Detect Multiple Myeloma," *Radiology*, vol. 306, no. 1, pp. 229–236, Jan. 2023, publisher: Radiological Society of North America. [Online]. Available: https://pubs.rsna.org/doi/full/10.1148/radiol.220311

[75] N. Ducros, J. F. P.-J. Abascal, B. Sixou, S. Rit, and F. Peyrin, "Regularization of nonlinear decomposition of spectral x-ray projection images," *Medical physics*, vol. 44, no. 9, pp. e174–e187, 2017.

[76] W. Zhang, N. Liang, Z. Wang, A. Cai, L. Wang, C. Tang, Z. Zheng, L. Li, B. Yan, and G. Hu, "Multi-energy ct reconstruction using tensor nonlocal similarity and spatial sparsity regularization," *Quantitative Imaging in Medicine and Surgery*, vol. 10, no. 10, p. 1940, 2020.

[77] W. Sun, B. Cui, Z. Lan, L. Li, X. Tang, X. Zhang, J. Ren, N. Liang, L. Lei, and Y. Bin, "Research on noise reduction technology of PCD spectral imaging based on Transformer," in *Proceedings of the 4th International Conference on Artificial Intelligence and Computer Engineering*, ser. ICAICE '23. New York, NY, USA: Association for Computing Machinery, May 2024, pp. 286–290. [Online]. Available: https://dl.acm.org/doi/10.1145/3652628.3652675

Appendix A

Supporting Data

Appendix B

Satirical Support